SANDIA REPORT

SAND2010-4763
Unlimited Release
Printed August 2010

A Modal Approach to Modeling Spatially Distributed Vibration Energy Dissipation

D.J. Segalman

Prepared by
Sandia National Laboratories
Albuquerque, New Mexico 87185 and Livermore, California 94550

Sandia National Laboratories is a multi-program laboratory managed and operated by Sandia Corporation, a wholly owned subsidiary of Lockheed Martin Corporation, for the U.S. Department of Energy's National Nuclear Security Administration under contract DE-AC04-94AL85000.
Approved for public release; further dissemination unlimited.

Issued by Sandia National Laboratories, operated for the United States Department of Energy by Sandia Corporation.

Available to DOE and DOE contractors from
U.S. Department of Energy
Office of Scientific and Technical Information
P.O. Box 62
Oak Ridge, TN 37831

Telephone: (865) 576-8401
Facsimile: (865) 576-5728
E-Mail: reports@adonis.osti.gov
Online ordering: http://www.osti.gov/bridge

Available to the public from
U.S. Department of Commerce
National Technical Information Service
5285 Port Royal Rd
Springfield, VA 22161

Telephone: (800) 553-6847
Facsimile: (703) 605-6900
E-Mail: orders@ntis.fedworld.gov
Online ordering: http://www.ntis.gov/help/ordermethods.asp?loc=7-4-0#online

SAND2010-4763
Unlimited Release
Printed August 2010

A Modal Approach to Modeling Spatially Distributed Vibration Energy Dissipation

Daniel J. Segalman
Sandia National Laboratories
P.O. Box 5800, Albuquerque, NM 87185-1393
djsegal@sandia.gov

Abstract

The nonlinear behavior of mechanical joints is a confounding element in modeling the dynamic response of structures. Though there has been some progress in recent years in modeling individual joints, modeling the full structure with myriad frictional interfaces has remained an obstinate challenge.

A strategy is suggested for structural dynamics modeling that can account for the combined effect of interface friction distributed spatially about the structure. This approach accommodates the following observations:

1. At small to modest amplitudes, the nonlinearity of jointed structures is manifest primarily in the energy dissipation - visible as vibration damping.
2. Correspondingly, measured vibration modes do not change significantly with amplitude.
3. Significant coupling among the modes does not appear to result at modest amplitudes.

The mathematical approach presented here postulates the preservation of linear modes and invests all the nonlinearity in the evolution of the modal coordinates. The constitutive form selected is one that works well in modeling spatially discrete joints.

When compared against a mathematical truth model, the distributed dissipation approximation performs well.

Acknowledgment

The author thanks his many colleagues for their useful discussions and suggestions. In particular Michael Starr, Mikhail Mesh, Michael Guthrie, and Michael Jew provided much perspective. Michael Starr and Michael Jew are particularly thanked for sharing their experimental insights - which provided confidence to this author. Mikhail Mesh pointed the author to the work of Ishlinskii and Palmov, absolutely necessary for a proper discussion of the literature.

Rarely is there a new idea of great significance that springs uniquely from the mind of a single genius; this is not such an idea. The notion of using modal coordinates of corresponding linear systems in modeling nonlinear processes is not new - it even has a history in structural dynamics [7],[13]. The contribution of this monograph is to show a mathematical development where this notion can be applied systematically to the dynamics of structures whose nonlinearities derive from the presence of mechanical joints.

The core idea of the work presented here had a long and gradual gestation and its birth was due to the observations and contributions of numerous other researchers in the author's Sandia environment. The idea began with a challenge from my manger in the late 1990's, Dr. David Martinez, to find a way to incorporate joint nonlinearities into the conventional tools of structural dynamics - specifically modal analysis. This would offer both model fidelity and model reduction. It was at that time that the basic idea presented here was discussed, but the press of other work prevented further development of that concept.

This concept was reintroduced in 2003 as one of the possible approaches for nonlinear model reduction in an LDRD proposal. Though that proposal did get funded, the concept was set aside again in order to pursue another interesting model reduction approach [21]. (See Appendix B for the part of that proposal relevant to this monograph and its mathematical implementation.)

Later, as part of an NNSA Campaign 6 study in 2005, Brian Resor of Sandia's vibration laboratory performed shaker tests on a complex structure having a multitude of joints and other frictional interfaces. These tests at resonance and at a multitude of amplitudes demonstrated energy dissipation that behaved as a power of the driving force amplitude. Dr. Michael J. Starr commented repeatedly on the "joint-like" nature of this modal response. It was that observation, along with repeated insightful and encouraging conversations with Dr. Starr, that got the author off the stick.

A final impetus was the creation of an NNSA ASC milepost (referring to the Advanced Simulation and Computing Program of the Department of Energy). Among the deliverables of that milepost was the implementation of this approach in the massively parallel struc-

tural dynamics code Salinas. The lead code developer, Dr. Garth Reese, imposed some requirements on the mathematical tools to be integrated into his code:

1. It should be possible for the user to specify which modes would be treated in a nonlinear manner.
2. It should be possible to apply this nonlinear treatment to subsystems only, if the analyst desires.
3. The user should be able to specify the treatment of the remaining part of system response - the kinematics orthogonal to those nonlinear modes - either modally or though system mass and stiffness matrices.
4. This nonlinear treatment of some modes should not preclude the use of discrete joint models as well.

The reader will see the results of Dr. Reese's helpful prodding in the body of this report.

Another illustration of the nature of good (and bad) ideas occurring at multiple times and places is the seminar talk that Mikhail Mesh gave when he visited Sandia in mid 2004. He also suggested the notion of representing the constitutive behavior of modal coordinates by Iwan models (called BPII models in the body of this monograph.) Just as was the case for the rest of the joint mechanics research team, M. Mesh did not have the opportunity to explore these ideas at that time.

This last example illustrates another point as well: good ideas are come by relatively easily. The development of those ideas into something useful often requires the efforts of a community. It is with that thought in mind that the author thanks the joint mechanics research community of Sandia National Laboratories.

Finally, the author thanks the members of his management team over the last decade for their support and their patience.

Contents

Appendix

List of Figures

List of Tables

Nomenclature

α Exponent in power-law relationship between amplitude of harmonic loading and resulting dissipation per cycle, page 17

$\alpha_{\mathcal{B}}$ A vector of modal coordinates for subsystem $\mathcal{B}$, page 25

χ Exponent in singularity that must be in BPII distribution ρ in order to predict power-law dissipation, page 17

ΔK $K_{\mathcal{B}}^0 - K_{\mathcal{B}}^\infty$, page 24

$[\Phi_{\mathcal{B}_N}\ \Phi_{\mathcal{B}_L}]$ Partition of $\Phi_{\mathcal{B}}$ such that $\Phi_{\mathcal{B}_N}$ consists for the H deformation modes associated with nonlinear constitutive behavior and $\Phi_{\mathcal{B}_L}$ consists of the remaining columns, page 25

$\mathcal{B}$ Name of a subsystem, page 23

$\Phi_{\mathcal{B}}$ the eigenvectors of the subsystem having mass and stiffness matrices $(M_{\mathcal{B}}, K_{\mathcal{B}}^0)$, page 25

$\Psi_{\mathcal{B}_N}$ $M_{\mathcal{B}}\Phi_{\mathcal{B}_N}$, page 27

$\rho()$ Distribution defining the properties of a BPII model, page 17

υ Coefficient in power-law relationship between amplitude of harmonic loading and resulting dissipation per cycle, page 17

C Linear damping matrix for full system, page 28

$C_{\mathcal{B}}$ The linear damping matrix of subsystem $\mathcal{B}$. This matrix does not reflect any contribution of the joints, page 23

$D(F_0)$ Dissipation resulting from imposed harmonic loading at amplitude F_0, page 17

$D(u_0)$ Dissipation resulting from imposed harmonic loading associated with imposed displacement of amplitude u_0, page 19

$F(t)$ Force applied to joint at time t, page 17

F_0 Amplitude of imposed harmonic load, page 17

$F_{\mathcal{B}}^J$ A vector of self-equilibrating, nonlinear joint forces. Note that because these are forces applied *by* the joint to the attached nodes, the sign is opposite to that of Equation 1.1 where forces are applied *to* the joint., page 23

$F_{\mathcal{B}}^{X}$ A vector of external loads applied to substructure $\mathcal{B}$, page 23

$f_k(\alpha_k(s))$ General nonlinear constitutive response associated with mode k, page 26

K Stiffness matrix for full system, page 28

$K_{\mathcal{B}}^{0}$ Tangent stiffness matrix for subsystem $\mathcal{B}$ about zero load, page 24

$K_{\mathcal{B}}^{\infty}$ The portion of the subsystem stiffness matrix left when joints are replaced by gaps, page 23

K_T Tangent stiffness of joint in the vicinity of zero load, page 18

M Mass matrix for full system, page 28

$M_{\mathcal{B}}$ Mass matrix of subsystem $\mathcal{B}$, page 23

P_n Projection matrix mapping displacements of the full system to to those of subsystem $\mathcal{B}_n$, page 28

$u(t)$ Displacement of joint at time t, page 17

u_0 Amplitude of joint displacement resulting form harmonic force of amplitude F_0, page 19

$u_{\mathcal{B}}$ Nodal (or generalized) displacements of subsystem $\mathcal{B}$, page 23

$x(t, \phi)$ a state variable capturing the history of joint deformation, page 17

BPII Bauschinger, Prandtl, Ishlinskii, Iwan - a class of constitutive model, page 16

Chapter 1

Introduction

There is a paradox of structural dynamics

1. On one hand experiment demonstrates distinct nonlinearity, particularly in the form of amplitude dependence of vibration damping.

2. On the other hand, linear analysis works well enough to be a practical tool so long as the damping parameters can be tuned to the structure and experiment at hand. (Different tuning is required for different experiments.)

The twin purposes of this monograph are to reconcile the above observations and to suggest an effective and efficient method of structural dynamics analysis that accommodates the observed nonlinearity.

Nonlinearity of Built-Up Structures

Recently there has been a renewed focus on mechanics of joints and the dynamics of built up structures. This renewed interest appears to derive from the desire to speed the design process and rely more on computational prediction and less on test. This is a particularly appealing strategy given the remarkable advances that have taken place in super computing in recent years.

The goal of predictive computer simulation of structural dynamics requires setting aside some of the simplifications that have been used in traditional engineering analysis, that required post test tuning (*knobs*). The most significant of these *knobs* in structural dynamics is modal damping, which must be calibrated for each mode for the level of excitation expected in the application to be modeled. Even with tuning, linear models are still incapable of capturing the damping of structures at high amplitude and continuing to model the damped behavior as the amplitude of vibration declines.

Features Common to Joints and to Jointed Structures

Mechanical joints and their role in vibration damping has been a topic of research interest for at least a century. (Extensive reviews can be found in [22] and [23]). Among the features found in tests of mechanical interfaces are

1. Under harmonic loading, joint dissipation per cycle increases approximately as a power of load amplitude and that power generally lies between 2.2 and 2.8.
2. Also under harmonic loading and modest load amplitudes, the effective stiffness decreases slightly with amplitude of excitation.
3. Though dissipation per cycle shows a strong dependence on load amplitude, it has little rate dependence.

The above behavior is suggested notionally in Figure 1.1.

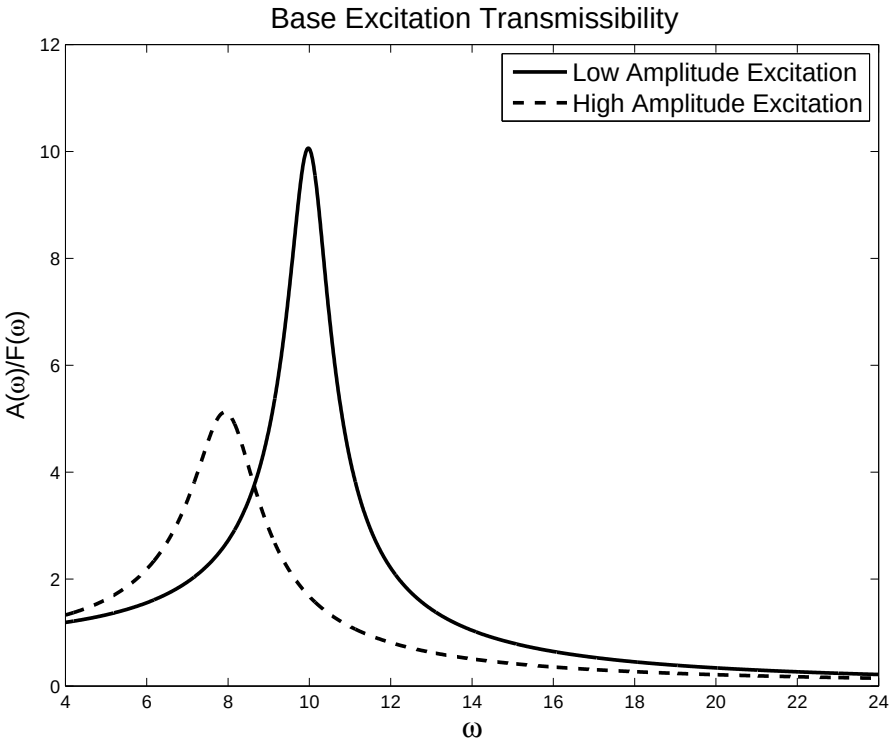

Figure 1.1. *Transmissibility of Base Excited System conveys qualitatively the behavior of individual joints.*

Actual experimental data of energy dissipation per cycle versus force is presented in Figure 1.2. The discrete points in these log-log plots are associate with harmonic axial

loading of simple lap joints at different levels of axial load. Cases of multiple clamping loads are considered and power law fits are found for each level of clamping load. Energy dissipation for the case of a monolithic (joint-free) specimen is also shown. In such cases, the energy dissipation is orders of magnitude less than that of jointed specimens and the power-law fit has a slope of approximately 2.0 - substantially less than for the cases of jointed specimens. This data, due to Danny L. Gregory, is found in [23].

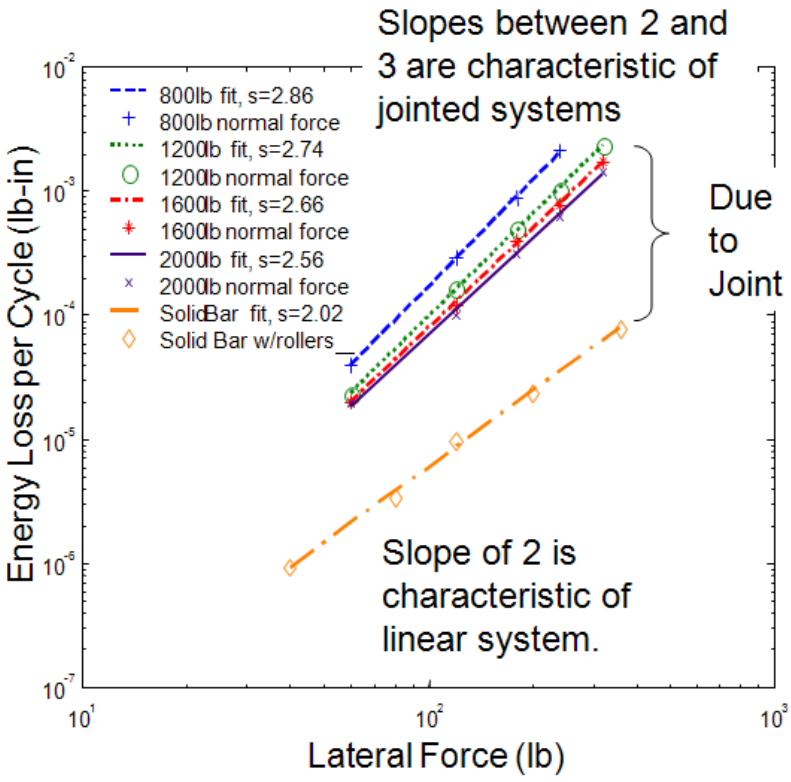

Figure 1.2. *Experimental Energy Dissipation of Steel-Steel Specimens.*

Computational Issues in Dynamics of Built-Up Structures

In general, a majority of the nonlinearity encountered in structural mechanics is due to nonlinearities at interfaces. There are several flavors of such nonlinearity including micro-slip, macro-slip, impact, and combinations of all. The problems considered in this formulation are ones where the magnitude of excitation is low enough that one does not expect impact or that many of the interfaces go into macro-slip.

A long history of modeling individual joints is marked by a recent flurry in development of new model forms and incorporation of those into structural dynamics code. Recent work in this area was brought together in focused workshops in 2006 [22] and 2009. (A report on the 2009 workshop is currently undergoing peer review.)

Modeling of Individual Joints and Incorporation of Joint Models in Finite Element Models

A class of constitutive model that has had some success in modeling mechanical joints is that associated with Bauschinger[1], Prandtl[18], Ishlinskii [9], and Iwan[11] and [10]. This model class (referred to in the following as the BPII class) has been used by the above authors primarily to capture the qualitative properties of metals under large deformation.

The BPII model class is consistent with the sketch in Figure 1.3 In that figure, each

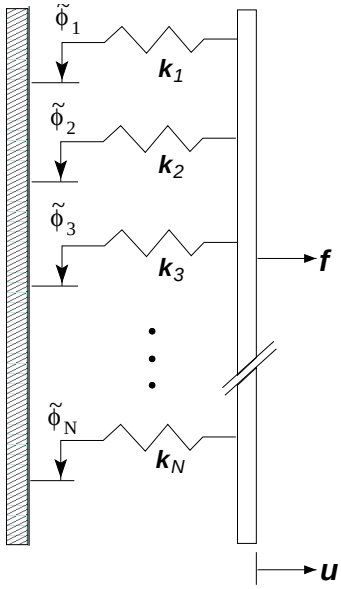

Figure 1.3. *The BPII model is consistently represented as an infinite parallel union of Jenkins elements.*

Jenkins element consists of a slider of strength $\tilde{\phi}_j$ and a spring of stiffness k_j. Combining results from [11], [27] and [26], one can show that such models can be represented through a change of variables without loss of generality by equivalent structures all having stiffness $k_j = 1$.

Mathematically, the model form is now expressed:

$$F(t) = \int_0^\infty \rho(\phi)[u(t) - x(t,\phi)]\, d\phi \tag{1.1}$$

where F is the force imposed on the joint; $u(t)$ is the joint displacement at time t; $\rho()$ is the distribution defining the properties of a BPII model; and

$$\dot{x}(t,\phi) = \begin{cases} \dot{u} & \text{if } \|u - x(t,\phi)\| = \phi \text{ and } \dot{u}(u - x(t,\phi)) > 0 \\ 0 & \text{otherwise} \end{cases} \tag{1.2}$$

is a state variable capturing the history of joint deformation. We are guaranteed that $\|u - x(t,\phi)\| \leq \phi$.

After the change of variables mentioned above, the quantities have dimensions as follows. "Dummy" parameter ϕ has dimensions of length. Distribution $\rho()$, which contains all joint parameterization,has dimensions of force/length^2. The dimensions of the external loads and displacements applied to the joint remain unchanged.

An instance of this class has been used extensively by Palmov [16] to capture the bulk response of metals to dynamic problems of large deformation. This model class has been used in more recent years also to model mechanical joints [17], [12], [27], and [20].

As discussed above, laboratory testing shows that for most frictional joints, when subjected to harmonic excitation of magnitude F_0, the resulting energy dissipation per cycle conforms to a power-law in F_0

$$D(F_0) = \upsilon F_0^\alpha \tag{1.3}$$

where $2 < \alpha < 3$ ([30],[31],[32],[6]).

One can show mathematically [26] that for the dissipation to behave in a power-law manner the corresponding distribution must be asymptotically

$$\rho(\phi) \approx R\phi^\chi \quad \text{for small } \phi \tag{1.4}$$

where

$$\chi = \alpha - 3 \tag{1.5}$$

Consideration of small deformations permits us to deduce that at *very* small deformation

$$F(t) = u(t) \int_0^\infty \rho(\phi)\, d\phi \tag{1.6}$$

providing us an expression for tangent stiffness at small load:

$$K_T = \int_0^\infty \rho(\phi)\, d\phi \tag{1.7}$$

Note that this demonstrates that admissible ρ must be integrable over the interval $(0, \infty)$.

Palmov's 3-Parameter Model

The simplest model that satisfies this condition is one where one explicitly considers only small loads and displacements. One assumes that the distribution function behaves as Equation 1.4 at small loads and that only small load information is available: power-law dissipation and low-load stiffness, K_T.

With small deformations in mind, we re-write Equation 1.1

$$F(t) = \int_0^\epsilon \rho(\phi)[u(t) - x(t,\phi)]\, d\phi + u \int_\epsilon^\infty \rho(\phi)\, d\phi \tag{1.8}$$

where ϵ is chosen to be a displacement so small that $\rho(u_0)$ is well approximated by $R\phi^\chi$ for $\phi < \epsilon$ but that the anticipated simulations or experiments will not cause displacements exceeding ϵ.

We may now write Equation 1.8 as

$$F(t) = K_T\, u(t) - \int_0^\epsilon \rho(\phi) x(t,\phi)\, d\phi = K_T\, u(t) - \int_0^\epsilon R\phi^\chi x(t,\phi)\, d\phi \tag{1.9}$$

$$= K_T\, u(t) - \int_0^\infty R\phi^\chi x(t,\phi)\, d\phi \tag{1.10}$$

since $x(t,\phi) = 0$ for all $\phi > \epsilon$. If one does perform simulations such that displacement exceeds ϵ, pathological behavior results. This model cannot be used to predict large load/deformation behavior of joints.

This three parameter (K_T, R, χ) BPII model is discussed extensively by Palmov [16] and appears to have been constructed so as to be mathematically equivalent to the Masing model explored much earlier by Davidenkov [4]. This same Iwan model was explored again much later by Segalman [26]. Interestingly enough, the Davidenkov Masing model was eventually rediscovered by Smallwood [29]. (A reasonably good discussion connecting Masing and Iwan models can be found in [25] and another discussion on using Iwan models to explore the connections among Masing models can be found in [28].)

At this point, it would be useful to discuss the process of deducing parameters for this model from experiment. The value of K_T is deduced from small load experiments in the

obvious manner and the value of χ is deduced from the slope of the dissipation power-law plot with the help of Equation 1.5. As discussed above and frequently in the literature (for instance, [16] , [26], [27]) the energy dissipation taking place in the joint per cycle in harmonic loading is

$$D(u_0) = \int_0^{u_0} 4\,[u_0 - \phi]\,\phi\rho(\phi)\,d\phi \tag{1.11}$$

where u_0 is the maximum displacement resulting from that harmonic loading.

Performing the relevant integration and matching the dissipation with that of Equation 1.3, we deduce that

$$R = \upsilon(2+\chi)(3+\chi)K_T^{3+\chi}/4 \tag{1.12}$$

The Sandia 4-Parameter Model

Another distribution that satisfies the character of Equation 1.4 but that also has meaning at large loads was presented and explored in [27]. That distribution has the form

$$\rho(\phi) = R\phi^{\chi}[H(\phi) - H(\phi - \phi_{\max})] + S\delta(\phi - \phi_{\max}) \tag{1.13}$$

where $H()$ is the Heaviside step function, δ is the Dirac delta function. The parameters $\phi_{\max}$ S and R can be expressed in terms of a preferred set of parameters:

- F_S is the force necessary to initiate macro-slip;
- K_T is the joint stiffness at small load;
- χ is as defined in Equation 1.5;
- β relates to the shape of the dissipation curve, where it deviates from strict power-law.

Parameter F_S has dimensions of force; K_T has dimensions of stiffness; and χ and β are dimensionless. Methods for extracting joint parameters from experimental data are discussed in [23].

The above 4-parameter model has been incorporated into the massively parallel structural dynamics finite element code Salinas [19]. In this implementation, the joint is a zero-volume, one-dimensional nonlinear element and very realistic predictions of the vibration of structures having a small number of discrete joints are obtained ([2] and [24]).

Of course, the Sandia 4-parameter model reduces to Palmov's three-parameter model when loads/deflections are restricted to very small values. These two constitutive model forms will be discussed further in the following.

Limitations Associated with Modeling Discrete Joints

The above work is reflective of major advances that have taken place over the last decade in developing constitutive models for joints and incorporating those models into structural dynamics codes. This approach is especially useful for cases where nonlinear dynamic response is dominated by a small number of joints in the major load path.

Still, there are major limitations with this approach.

1. The most significant difficulty is that of obtaining the necessary parameterization for every joint in the structure. The experimental process of performing the necessary tests on each joint is discussed in detail in [23]. Alternatively one could perform fine-mesh-finite-element simulations of each joint and employ some sort of calibration correcting for the limitations of the relevant friction model. These laboratory or simulation results must be processed to obtain parameters for the relevant joints models.

   The exhausting process of obtaining parameters for just a few individual joints - particularly considering the part-to-part variability - precludes the prospect of modeling every joint individually in a complex structure.

2. The above discrete joint models are still pretty primitive. Among other limitations, they are intrinsically one-dimensional. Some computational [8] work and some experimental explorations [5] argue that joint response is fundamentally three-dimensional.

   Though one-dimensional models are being generalized to three dimensional form in innumerable ways (for instance using a formalism such as that introduced by Mröz [14]), accurate models will require both the development of advanced experimental techniques and extensive exploitation of those techniques to populate models for all of the relevant joints.

3. Just as creating test specimens for every joint type, material, geometry, and loading of interest and then performing multiple laboratory measurements on each is prohibitive; once having all of the resulting parameters, incorporating the myriad discrete joints into the relevant finite element model for the structure would likely be intractable also.

4. Interestingly, it appears that the more fidelity that a model has to capture the behavior that joints manifest in laboratory testing, the more difficult the resulting structural dynamics model is to solve. This difficulty is discussed below.

   A typical hysteresis loop for a BPII type model is shown in Figure 1.4. Though the symmetry relations are those that are used to define generalized Masing models [3], it has been demonstrated mathematically that the Masing class and the class of BPII models are mathematically equivalent [25].

   As loads increase, the hysteresis loop grows along both dimensions. Additionally, at small loads, the hysteresis loop has the shape of almost a straight line (limiting elastic behavior), and the loop opens up as loads increase. As a result, at large loads there is

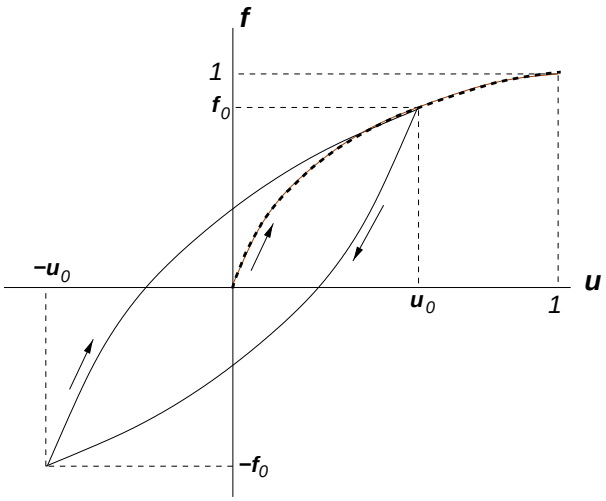

Figure 1.4. *Hysteresis loop of a Masing model.*

a discontinuity in instantaneous stiffness at load reversals (the upper right and lower left corners of the figure.)

This strong nonlinearity can excite very small amplitude high-frequency resonances which are not actually relevant to the engineering problem. The combination of high frequency and strong nonlinearity tends to drive down the time step that must be employed to make the resulting Newton iterations converge. Thus incorporating high fidelity discrete models for joints can increase the computational cost of analysis dramatically.

Proposed Approach to Distributed Nonlinearity

The notion presented here is fairly elementary; it rests on the following observations:

- Even under loads sufficient to cause structures to manifest significant nonlinearity - amplitude-dependent damping and apparent softening - linear eigenmodes[1] generally appear to be preserved. This is illustrated by the success of spatial filtering even beyond the linear regime.

- Coupling among the modes generally does not appear to become significant until very high loads. (Violation of this is most easily observed when modes appear to be complex.)

[1]The common arguement about whether to employ a hyphen or a space after the prefix "eigen" is resolved in this document by using neither. Such is the guidance found in [15].

- By segregating response modally, we may choose to treat only a subset of those modes (presumably those for which we have some data) in a nonlinear manner and to treat the remainder more conventionally.

At its simplest, the approach proposed here is to make the following postulates:

1. Modal forces excite only corresponding modal responses.
2. Modal coordinates evolve according to some simple nonlinear constitutive model.
3. The nonlinear modal constitutive response resolves to linear in the limit of small loads.

Given the above assumptions, we select a consistent constitutive model form that also reproduces the power-law dissipation seen on built up structures.

Chapter 2

Derivations

We are interested in modeling the structure in a manner that preserves the mode shapes and attaches a nonlinear behavior to at least some subset of those modes. Additionally, we would like to be able to perform this model reduction on a substructure and then to integrate this model into the full system model. We begin with the substructure model.

Nonlinear Distributed Damping of a Substructure

Consider a substructure labeled $\mathcal{B}$ (Figure 2.1), having

- mass matrix $M_{\mathcal{B}}$,
- linear damping matrix $C_{\mathcal{B}}$ (none of the joint damping is reflected in this matrix.)
- linearized stiffness matrix $K^0_{\mathcal{B}}$. This is the stiffness matrix that would be deduced from measurements taken at extremely low levels of excitation.

Initial Spatial Formulation for Substructure

The governing equation is

$$M_{\mathcal{B}}\ddot{u}_{\mathcal{B}} + C_{\mathcal{B}}\dot{u}_{\mathcal{B}} + K^{\infty}_{\mathcal{B}}u_{\mathcal{B}} = F^X_{\mathcal{B}} + F^J_{\mathcal{B}} \tag{2.1}$$

where

- $u_{\mathcal{B}}$ are nodal displacements associated with subsystem $\mathcal{B}$,
- $M_{\mathcal{B}}$ and $C_{\mathcal{B}}$ are the mass and linear damping matrices of the substructure, respectively. The damping matrix is associated with linear damping processes (the resulting dissipation being quadratic in veleocity components), so it does not capture the dissipation due to joints.

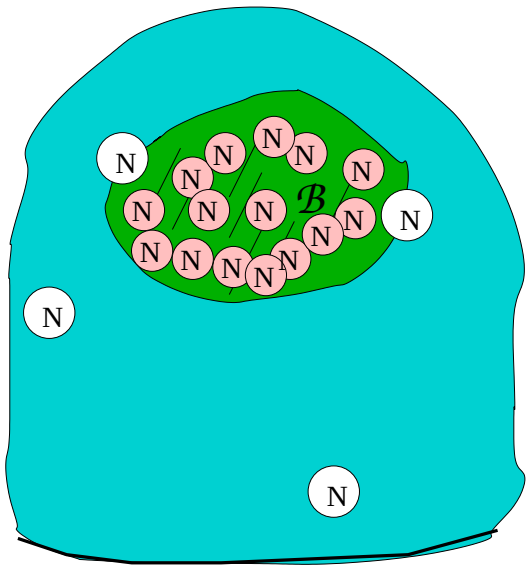

Figure 2.1. em Substructure $\mathcal{B}$ contains linear and nonlinear components. Its connection to the full system may involve discrete nonlinearities and there my be nonlinearities distributed elsewhere in the structure.

- $K_{\mathcal{B}}^{\infty}$ is the stiffness matrix of the substructure that would be measured if all joints were disconnected;
- $F_{\mathcal{B}}^{J}$ is a vector of self-equilibrating, nonlinear joint forces. Note that because these are forces applied *by* the joint to the attached nodes, the sign is opposite to that of Equation 1.1 where forces are applied *to* the joint
- and $F_{\mathcal{B}}^{X}$ is a vector of external loads

One part of $F_{\mathcal{B}}^{J}$ is the zero-load linearization

$$F_{\mathcal{B}}^{J} = -\Delta K_{\mathcal{B}}\, u_{\mathcal{B}} + \Delta F_{\mathcal{B}}^{J} \tag{2.2}$$

Adding $\Delta K_{\mathcal{B}}\, u_{\mathcal{B}}$ to Equation 2.1 and defining

$$K_{\mathcal{B}}^{0} = K_{\mathcal{B}}^{\infty} + \Delta K_{\mathcal{B}} \tag{2.3}$$

the low-load stiffness of the subsystem, we obtain the governing equation

$$M_{\mathcal{B}}\ddot{u}_{\mathcal{B}} + C_{\mathcal{B}}\dot{u}_{\mathcal{B}} + K_{\mathcal{B}}^{0}u_{\mathcal{B}} = F_{\mathcal{B}}^{X} + \Delta F_{\mathcal{B}}^{J} \tag{2.4}$$

Modal Formulation for Substructure

Let $\Phi_{\mathcal{B}}$ be the matrix whose columns are the eigenvectors of the $(M_{\mathcal{B}}, K^0_{\mathcal{B}})$ system above. We define modal coordinates in body $\mathcal{B}$ and use the matrix $\Phi_{\mathcal{B}}$ to map them to spatial degrees of freedom:

$$u_{\mathcal{B}} = \Phi_{\mathcal{B}} \alpha_{\mathcal{B}} \tag{2.5}$$

where $\alpha_{\mathcal{B}}$ is a vector of modal coordinates. Here and in the following, $\Phi_{\mathcal{B}}$ contains *all* the eigenvectors of the subsystem, but it will develop that not all of them actually need to be calculated. Also, we assume that the eigenvectors are mass normalized

$$\Phi^T_{\mathcal{B}} M_{\mathcal{B}} \Phi_{\mathcal{B}} = I \tag{2.6}$$

so pre-contracting Equation 2.5 with $\Phi^T_{\mathcal{B}} M_{\mathcal{B}}$, we obtain:

$$\alpha_{\mathcal{B}} = \Phi^T_{\mathcal{B}} M_{\mathcal{B}} u_{\mathcal{B}} \tag{2.7}$$

We pre-contract Equation 2.4 by Φ^T to diagonalize the linear system:

$$\left[\Phi^T_{\mathcal{B}} M_{\mathcal{B}} \Phi_{\mathcal{B}}\right] \ddot{\alpha}_{\mathcal{B}} + \left[\Phi^T_{\mathcal{B}} C_{\mathcal{B}} \Phi_{\mathcal{B}}\right] \dot{\alpha}_{\mathcal{B}} + \left[\Phi^T_{\mathcal{B}} K^0_{\mathcal{B}} \Phi_{\mathcal{B}}\right] \alpha_{\mathcal{B}} = \Phi^T_{\mathcal{B}} F^X_{\mathcal{B}} + \Phi^T_{\mathcal{B}} \Delta F^J_{\mathcal{B}} \tag{2.8}$$

$$\ddot{\alpha}_{\mathcal{B}} + \mathrm{diag}\left(\{2\zeta_k \omega_k\}\right) \dot{\alpha}_{\mathcal{B}} + \mathrm{diag}\left(\left\{\omega_k^2\right\}\right) \alpha_{\mathcal{B}} = \Phi^T_{\mathcal{B}} F^X_{\mathcal{B}} + \Phi^T_{\mathcal{B}} \Delta F^J_{\mathcal{B}} \tag{2.9}$$

Note that we have assumed modal damping for the linear portion of the model.

Enabling Simplifications

Let's introduce **Simplifying Assumption 1:** *The joint forces project only onto the first H eigen modes.* Mathematically, we express this by decomposing the modal matrix

$$\Phi_{\mathcal{B}} = [\Phi_{\mathcal{B}_N} \, \Phi_{\mathcal{B}_L}] \tag{2.10}$$

where $\Phi_{\mathcal{B}_N}$ consists of the H deformation modes to which we intend to ascribe nonlinear constitutive behavior and $\Phi_{\mathcal{B}_L}$ consists of the remaining columns. We assert that

$$\Phi^T_{\mathcal{B}} \left(\Delta K u_{\mathcal{B}} + F^J_{\mathcal{B}}\right) = \begin{bmatrix} \Phi^T_{\mathcal{B}_N} \\ \Phi^T_{\mathcal{B}_L} \end{bmatrix} \Delta F^J_{\mathcal{B}} = \begin{bmatrix} \Phi^T_{\mathcal{B}_N} \Delta F^J_{\mathcal{B}} \\ 0 \end{bmatrix} \tag{2.11}$$

Let's now postulate **Simplifying Assumption 2:** *The joint forces in Equation 2.9 have a diagonal form*

$$\Phi_{\mathcal{B}_N}^T \Delta F_{\mathcal{B}}^J = \left\{ f_k(\alpha^k(s), s = -\infty \text{ to } t) \right\} \tag{2.12}$$

Specifically, the k^{th} nonlinear modal force depends only on the history of the corresponding modal displacement.

The dynamic equations for the subsystem in modal coordinates are now

$$\ddot{\alpha}_{\mathcal{B}} + \text{diag}\left(\{2\zeta_k\omega_k\}\right)\dot{\alpha}_{\mathcal{B}} + \text{diag}\left(\left\{\omega_k^2\right\}\right)\alpha_{\mathcal{B}} = \Phi_{\mathcal{B}}^T F_{\mathcal{B}}^X + \begin{bmatrix} \left\{ f_k(\alpha^k(s), s = -\infty \text{ to } t) \right\} \\ 0 \end{bmatrix} \tag{2.13}$$

where the column vector on the right hand side is nonzero only for terms associated with the H nonlinearly evolving modes.

Transferring back to nodal degrees of freedom (using Equation 2.7 to express α_B in terms of $u_{\mathcal{B}}$):

$$\Phi_{\mathcal{B}}^T M_{\mathcal{B}} \ddot{u}_{\mathcal{B}} + \text{diag}\left(\{2\zeta_k\omega_k\}\right)\Phi_{\mathcal{B}}^T M_{\mathcal{B}} \dot{u}_{\mathcal{B}} + \text{diag}\left(\left\{\omega_k^2\right\}\right)\Phi_{\mathcal{B}}^T M_{\mathcal{B}} u_{\mathcal{B}}$$

$$= \Phi_{\mathcal{B}}^T F_{\mathcal{B}}^X + \begin{bmatrix} \left\{ f_k(\alpha^k(s), s = -\infty \text{ to } t) \right\} \\ 0 \end{bmatrix} \tag{2.14}$$

Pre-contracting by $M_{\mathcal{B}}\Phi_{\mathcal{B}} = \Phi_{\mathcal{B}}^{-T}$

$$M_{\mathcal{B}} \ddot{u}_{\mathcal{B}} + \Phi_{\mathcal{B}}^{-T}\text{diag}\left(\{2\zeta_k\omega_k\}\right)\Phi_{\mathcal{B}}^{-1} \dot{u}_{\mathcal{B}} + \Phi_{\mathcal{B}}^{-T}\text{diag}\left(\left\{\omega_k^2\right\}\right)\Phi_{\mathcal{B}}^{-1} u_{\mathcal{B}}$$

$$= F_{\mathcal{B}}^X + M_{\mathcal{B}}\Phi_{\mathcal{B}} \begin{bmatrix} \left\{ f_k(\alpha^k(s), s = -\infty \text{ to } t) \right\} \\ 0 \end{bmatrix} \tag{2.15}$$

observing that

$$\Phi_{\mathcal{B}}^{-T}\text{diag}\left(\{2\zeta_k\omega_k\}\right)\Phi_{\mathcal{B}}^{-1} = C_{\mathcal{B}} \tag{2.16}$$

$$\Phi_{\mathcal{B}}^{-T}\text{diag}\left(\left\{\omega_k^2\right\}\right)\Phi_{\mathcal{B}}^{-1} = K_{\mathcal{B}}, \tag{2.17}$$

$$M_{\mathcal{B}}\Phi_{\mathcal{B}} = [M\Phi_{\mathcal{B}_N} \quad M\Phi_{\mathcal{B}_L}] \tag{2.18}$$

the equation of motion for the subsystem is now

$$M_{\mathcal{B}}\ddot{u}_{\mathcal{B}} + C_{\mathcal{B}}\dot{u}_{\mathcal{B}} + K_{\mathcal{B}}u_{\mathcal{B}} = F^X_{\mathcal{B}} + \left[\begin{array}{c} \Psi^T_{\mathcal{B}_N} \left\{ f_k(\alpha^k(s), s = -\infty \text{ to } t) \right\} \\ 0 \end{array} \right] \tag{2.19}$$

where

$$\Psi_{\mathcal{B}_N} = \Phi^T_{\mathcal{B}_N} M_{\mathcal{B}} \tag{2.20}$$

Any reasonable constitutive equation could be used to capture the modal nonlinearity, but since BPII models have been successful in capturing the behavior of discrete joints, it is a natural **Constitutive Assumption** that nonlinear modal force is also described by a BPII model.

$$\begin{aligned} \Phi^T_{\mathcal{B}_N} \Delta F^J_{\mathcal{B}} \quad &= \quad \left\{ f_k(\alpha^k(s), s = -\infty \text{ to } t) \right\} \\ &= \int_0^\infty \text{diag}\left(\{\rho_k(\phi)\} \right) \beta(t, \phi) d\phi \end{aligned} \tag{2.21}$$

where

$$\dot{\beta}^k(t, \phi) = \begin{cases} \dot{\alpha}_k & \text{where} \quad \dot{\alpha}_k \left(\alpha^k - \beta^k \right) > 0 \quad \text{and} \quad \left| \alpha^k - \beta^k \right| = \phi \\ 0 & \text{otherwise} \end{cases} \tag{2.22}$$

The length of vector β is H and there will be H sets of constitutive parameters required for that many ρ_k.

Integration into Full Structure

Let's now introduce that subsystem damping into a full-system model.

Letting the nodal degrees of freedom of the full system be u, the governing equation is

$$\begin{aligned} &M\ddot{u} + C\dot{u} + Ku \\ &\quad = F^X + F^J_D + \sum_n P^T_n \, \Psi^T_{\mathcal{B}_N, n} \int_0^\infty \text{diag}\left(\{\rho_{k,n}(\phi)\} \right) \beta_n(t, \phi) d\phi \end{aligned} \tag{2.23}$$

where M, K, and C are full system matrices, vector F^J_D is the response of any discretely modeled joints not in any subsystem $\mathcal{B}_n$, and F^X is a vector of exteriorly applied loads

and summation takes place over all subsystems. Operator P_n is the projection matrix of displacements from the full system to those of subsystem $\mathcal{B}_n$.

$$u_{B,n} = P_n u \tag{2.24}$$

The coordinates of the nonlinearly evolving subsystem modes are

$$\alpha_{N,n} = \Psi^T_{\mathcal{B}_{N,n}} u_{\mathcal{B},n} = \Psi^T_{\mathcal{B}_{N,n}} P_n \, u \tag{2.25}$$

These modal coordinates are used to integrate the state functions β as indicated in Equation 2.22.

Chapter 3

Numerical Verification Calculations at Low Amplitude

Two-Mass System

Consider the toy problem indicated in Figure 3.1 consisting of two equal masses (M_0 each) connected by a spring of stiffness K_∞ and a nonlinear element.

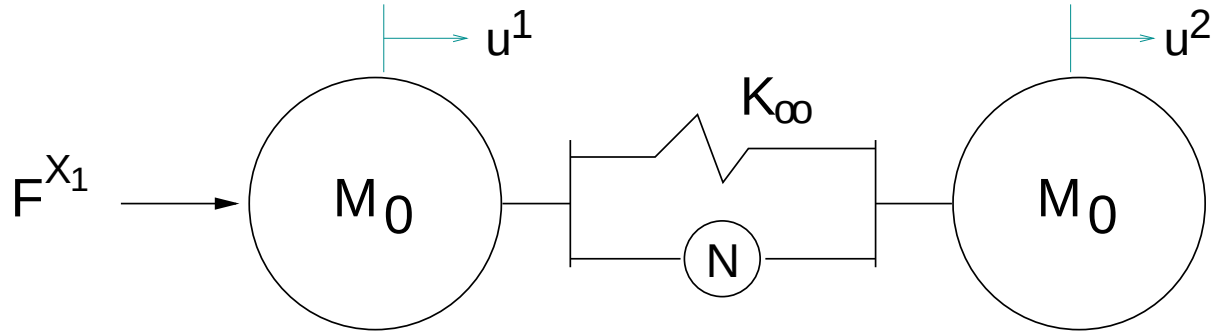

Figure 3.1. *Kinematics of a Two-Mass System.*

Governing Equations

The governing equations for this system are written in matrix form:

$$M_0 \begin{bmatrix} 1 & \\ & 1 \end{bmatrix} \begin{Bmatrix} \ddot{u}^1 \\ \ddot{u}^2 \end{Bmatrix} = -K^\infty \begin{bmatrix} 1 & -1 \\ -1 & 1 \end{bmatrix} \begin{Bmatrix} u^1 \\ u^2 \end{Bmatrix} + F_N \begin{Bmatrix} -1 \\ 1 \end{Bmatrix} + F^{X_1} \begin{Bmatrix} 1 \\ 0 \end{Bmatrix} \tag{3.1}$$

where F^{X_1} is the externally applied load on the left hand side and $F^J = F_N \left[-1\, 1\right]^T$ is the vector of forces that the joints apply to the masses.

Direct Solution of Two-Mass System

We consider the problem shown in Figure 3.1 where the externally applied load is

$$F^{X_1}(t) = A\,[H(t) - H(t - \pi/\omega)]\sin(\omega t) \tag{3.2}$$

where the excitation frequency ω is chosen to be the highest eigenfrequency of the elastic system and the nonlinear component is represented by the 4-parameter Iwan model. A numerical solution for Equation 3.1 can be obtained by use of Hilber, Hughes, Taylor integration using Newton iteration at each time step. The parameters for this problem are shown in Table 3.1.

Table 3.1. Parameters for Numerical Simulation

$M_0 = 10$	$K_\infty = 9$	$A = 500$	$\omega = \sqrt{2}$
$K_T = 1$	$F_S = 10$	$\chi = -0.5$	$\beta = 5$

The imposed load, the mean system velocity , and the relative acceleration are shown in Figure 3.2

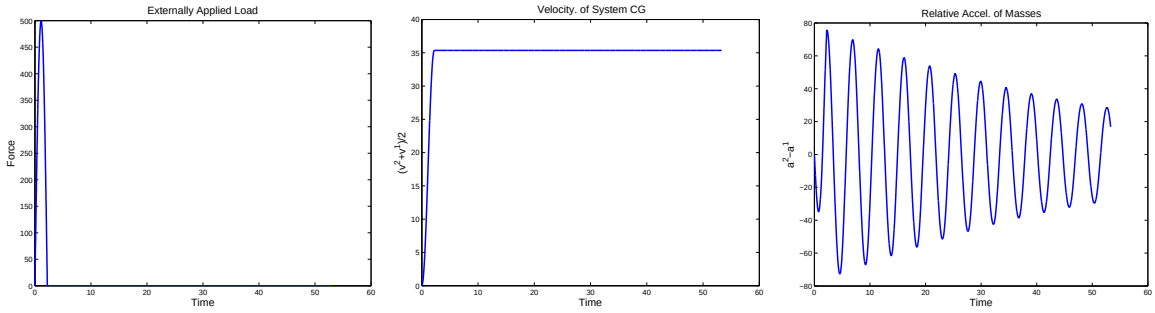

Figure 3.2. *Imposed load, resulting mean acceleration, and relative accelerations found from direction integration.*

Linearized System & Modal Coordinates

In the manner discussed in the subsection *Initial Spatial Formulation for Substructure* on page 23, Equation 3.1 can be put into the form of Equation 2.4.

$$M_0 \begin{bmatrix} 1 & \\ & 1 \end{bmatrix} \begin{Bmatrix} \ddot{u}^1 \\ \ddot{u}^2 \end{Bmatrix} + (K_\infty + K_T) \begin{bmatrix} 1 & -1 \\ -1 & 1 \end{bmatrix} \begin{Bmatrix} u^1 \\ u^2 \end{Bmatrix}$$

$$= \Delta F_N(u^2 - u^1) \left\{ \begin{array}{c} -1 \\ 1 \end{array} \right\} + \left\{ \begin{array}{c} F^{X_1} \\ 0 \end{array} \right\} \tag{3.3}$$

where $\Delta F_N(u^2 - u^1) = F_N(u^2 - u^1) + K_T(u^2 - u^1)$.

The left-hand side of Equation 3.3 is *the* linear approximation for the two-mass system about zero-load.

In the following, we shall employ eigenmodes of this elastic problem in evaluating the joint forces on the right hand side of Equation 3.3. This will involve joint-type evolution equations employing modal rather than spatial coordinates. Further, this is one of the few problems for which we can deduce readily the parameters for those modal oriented joint equations.

In this problem (and in the more complicated ones ahead) each of the modal responses is represented by the system in Figure 3.3. This is a four-parameter Iwan system in parallel with a spring; there are five parameters to find. In the following we discuss how these parameters can be deduced for this simple problem.

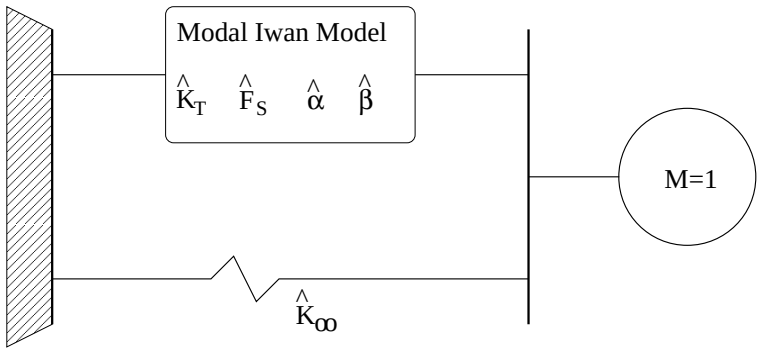

Figure 3.3. *The modal response is represented as a 4-parameter Iwan model in parallel with a spring. There are a total of five parameters for each modal model.*

We shall need the eigenmodes of this elastic system and we proceed in the standard manner. The linear homogeneous system has the following eigenequation

$$\left(\omega^2 \left[\begin{array}{cc} 1 & \\ & 1 \end{array} \right] - \omega_0^2 \left[\begin{array}{cc} 1 & -1 \\ -1 & 1 \end{array} \right] \right) \left\{ \begin{array}{c} y^1 \\ y^2 \end{array} \right\} = \left\{ \begin{array}{c} 0 \\ 0 \end{array} \right\} \tag{3.4}$$

where $\omega_0^2 = K_0/M_0$ and $K_0 = K_\infty + K_T$.

This has eigensolutions

$$\omega_1^2 = 0 \quad \text{and} \quad y^1 = \tfrac{1}{\sqrt{2M_0}} \left\{ \begin{array}{c} 1 \\ 1 \end{array} \right\} \tag{3.5}$$

and

$$\omega_2^2 = 2\omega_0^2 \quad \text{and} \quad y^2 = \tfrac{1}{\sqrt{2M_0}} \left\{ \begin{array}{c} -1 \\ 1 \end{array} \right\} \tag{3.6}$$

In the usual manner, we now represent the physical degrees of freedom in terms of modal coordinates

$$\left\{ \begin{array}{c} u^1 \\ u^2 \end{array} \right\} = \Phi \left\{ \begin{array}{c} \alpha^1 \\ \alpha^2 \end{array} \right\} \tag{3.7}$$

where

$$\Phi = \gamma \left[\begin{array}{cc} 1 & -1 \\ 1 & 1 \end{array} \right] \tag{3.8}$$

and

$$\gamma = \frac{1}{\sqrt{2M_0}} \tag{3.9}$$

Similarly, we can represent the modal coordinates in terms of the physical coordinates:

$$\alpha = \Psi u \tag{3.10}$$

where from Equation 2.20

$$\Psi = \Phi^T \left[\begin{array}{cc} M_0 & \\ & M_0 \end{array} \right] = \frac{1}{2\gamma} \left[\begin{array}{cc} 1 & 1 \\ -1 & 1 \end{array} \right] \tag{3.11}$$

Because the first eigensolution is a rigid-body mode, only deformations aligned with the second mode contribute to ΔF_N response.

$$\alpha^2 = \Psi_{2,k} u^k = \frac{1}{2\gamma} \left(u^2 - u^1 \right) \tag{3.12}$$

If the physical joint force is $f = \Delta F_N \{-1 \quad 1\}^T$

$$\psi = \Phi^T f = \left\{ \begin{array}{c} 0 \\ 2\gamma \Delta F_N \end{array} \right\} \tag{3.13}$$

But also

$$\psi = \left\{ \begin{array}{c} 0 \\ \Delta \hat{F}_N(\alpha^2) \end{array} \right\} \tag{3.14}$$

Equating the components of the modal force vectors, we conclude that

$$\Delta \hat{F}_N(\alpha^2) = 2\gamma \, \Delta F_N(u^2 - u^1) = 2\gamma \, \Delta F_N(2\gamma\alpha^2) \tag{3.15}$$

showing that $\hat{F}_N$ and F_N have the same form. In fact, $\hat{F}_N$ is F_N scaled both in argument and magnitude.

Equations 3.15 and 3.12 are sufficient to deduce the parameters $[\hat{\chi}, \hat{\beta}, \hat{K_T}, \hat{F_S}]$ of a modal 4-parameter Iwan model from the corresponding parameters $[\chi, \beta, K_T, F_S]$ of a 4-parameter Iwan model employing physical coordinates. First, noting that $\hat{\rho}$ is a linear scaling of ρ and its augment, the two curves must have the same shape. From the above we assert that

1. $\hat{\chi} = \chi$ to preserve the shape of ρ.
2. $\hat{\beta} = \beta$ also to preserve the shape of ρ.
3. $\hat{F_S} = (2\gamma) F_S$ from Equation 3.15.
4. $\hat{K_T} = (2\gamma)^2 \, K_T$ from Equations 3.12 and 3.15.
5. $\hat{K_\infty} = (2\gamma)^2 \, K_\infty$ is deduced using reasoning similar to that of the previous step.

(Note that these relationships also fall out of the results of Appendix B.)

We evaluate the joint force term on the right hand side of Equation 3.3

$$\Delta F_N(u^2 - u^1) \left\{ \begin{array}{c} -1 \\ 1 \end{array} \right\} = \Psi^T \left[\Delta \hat{F}_N \left(\frac{u^2 - u^1}{2\gamma} \right) \left\{ \begin{array}{c} 0 \\ 1 \end{array} \right\} \right] = \frac{1}{2\gamma} \Delta \hat{F}_N \left(\frac{u^2 - u^1}{2\gamma} \right) \left\{ \begin{array}{c} -1 \\ 1 \end{array} \right\} \tag{3.16}$$

Numerical Solution With Modal Coordinates

The equations of motion, employing Equation 3.16 were solved numerically and for the same case as in subsection *Direct Solution of Two-Mass System* on page 30. The imposed load and the resulting mean system velocity and the relative acceleration of the two masses are plotted in Figure 3.4.

We see that the results of these two approaches are identical.

With the little bit of confidence gained from this problem, we go on to a problem that tests the method of distributed damping of a subsystem of a larger structure.

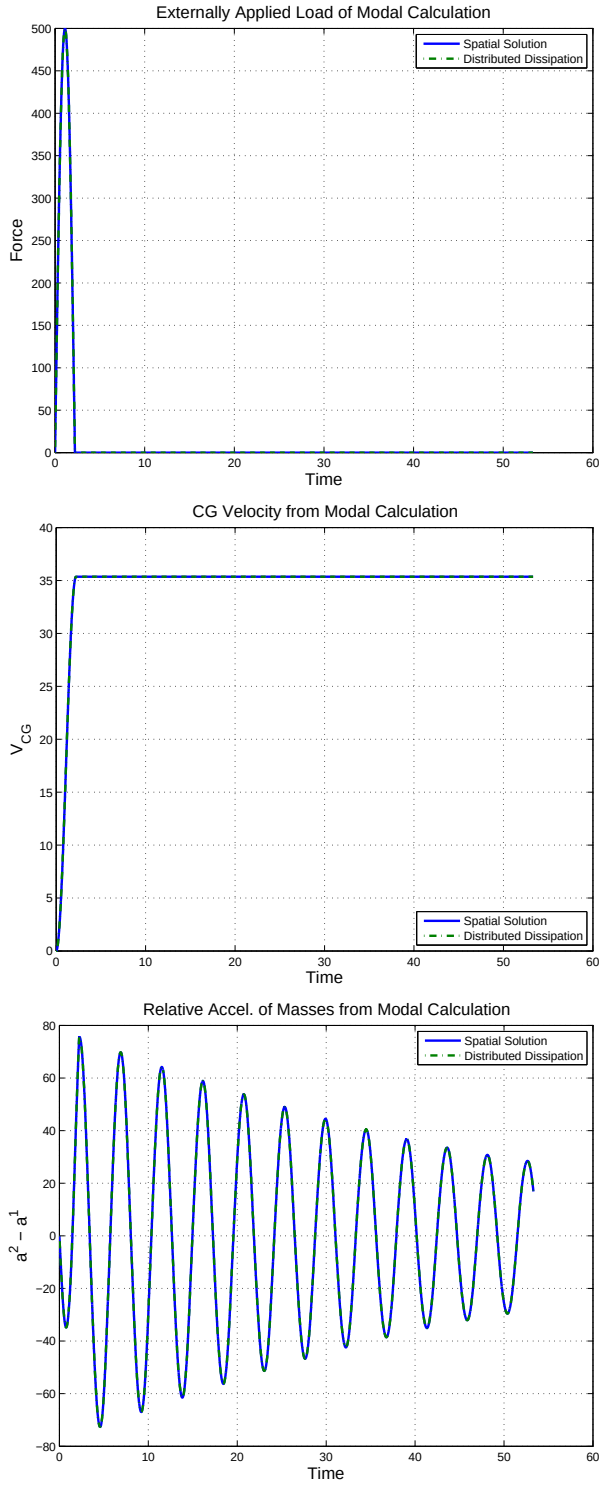

Figure 3.4. *Imposed load, velocity of center of gravity, and relative accelerations for the 2-mass system found from numerical solution of the formalism including modal joint dissipation. Also shown is the spatial solution.*

Three-Mass System

We consider the system shown in Figure 3.5.

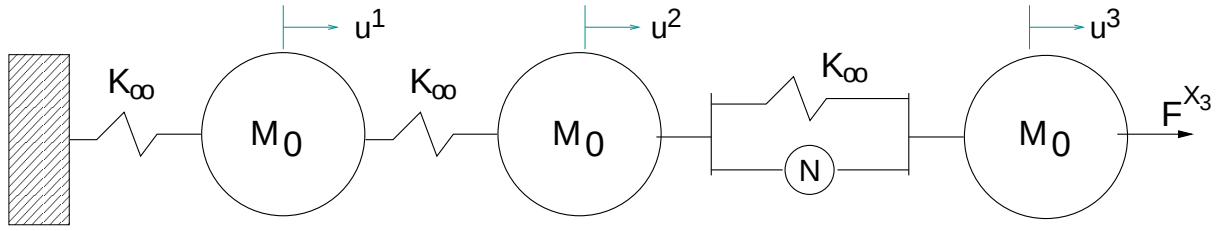

Figure 3.5. *Kinematics of a Three-Mass System, of which the previous system is a part.*

As in the previous section, we first solve this problem directly and then again using the method of distributed damping. The problem parameters are those shown in Table 3.1, but with the excitation frequency chosen to be $\omega = 1.74$, the highest eigenfrequency of the linear system.

The governing equation has the form

$$M\ddot{u} + Ku = F^X + F^J \tag{3.17}$$

where

$$M = \begin{bmatrix} M_0 & & \\ & M_0 & \\ & & M_0 \end{bmatrix} \quad \text{and} \quad K = \begin{bmatrix} 2K_\infty & -K_\infty & \\ -K_\infty & 2K_\infty & -K_\infty \\ & -K_\infty & K_\infty \end{bmatrix} \tag{3.18}$$

$$F^J = F_N \begin{Bmatrix} 0 \\ 1 \\ -1 \end{Bmatrix} \quad \text{and} \quad F^X = F_x \begin{Bmatrix} 0 \\ 0 \\ 1 \end{Bmatrix} \tag{3.19}$$

Solution Fully in Physical Coordinates

An integration of Equation 3.17 using only physical coordinates resulted in the plots for imposed load, acceleration of center mass, and relative displacements of the third and second masses shown in Figure 3.6.

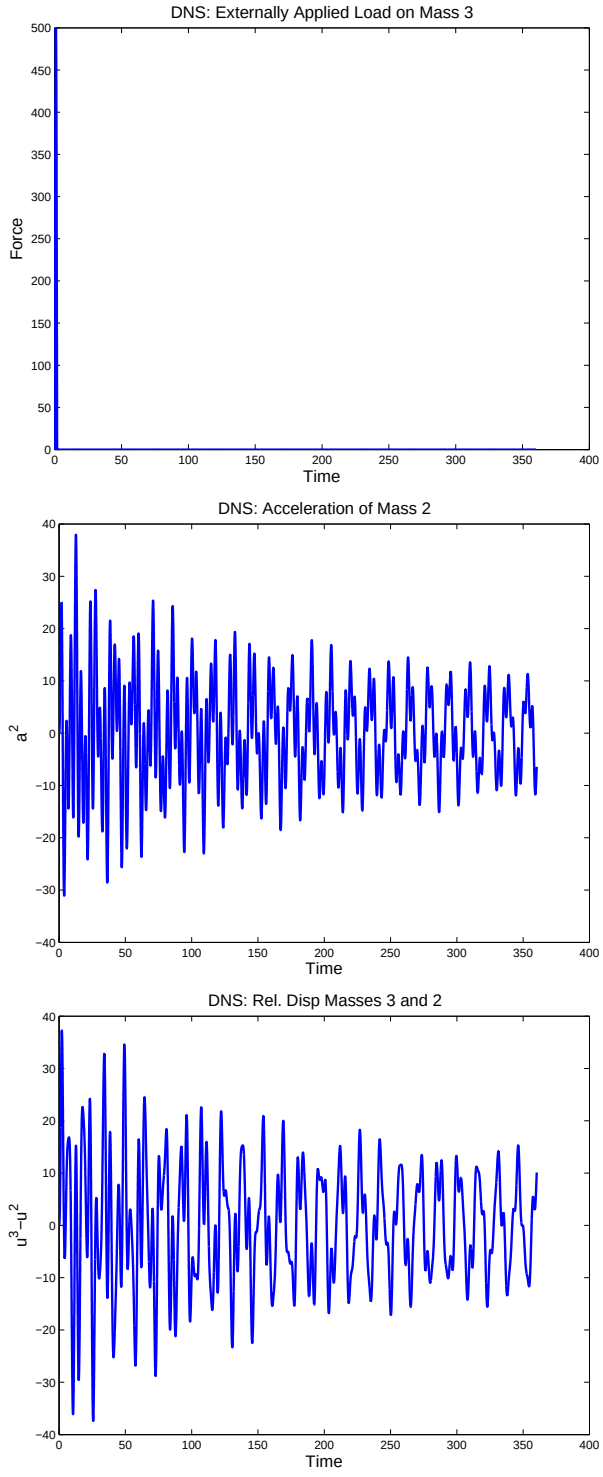

Figure 3.6. *Imposed load, acceleration of center mass, and relative displacements of the third and second masses found from direction integration of the three-mass problem.*

Solution Using Modal Distributed Damping

Here we recognize that the two masses on the right hand side of the structure and the connections between them are exactly the system examined in Section *Two-Mass System* beginning on page 29. In the following, we employ the modal expression for the nonlinear part of this subsystem in our analysis of the full system.

In the context of the three-mass problem, Equation 2.4 is:

$$M\ddot{u} + K_0 u = F^X + \Delta F^J \tag{3.20}$$

where

$$K_0 = \begin{bmatrix} 2K_\infty & -K_\infty & \\ -K_\infty & 2K_\infty + K_T & -K_\infty - K_T \\ & -K_\infty - K_T & K_\infty + K_T \end{bmatrix} \tag{3.21}$$

Because the modal formulation for distributed damping employs subsystem coordinates, we must introduce the transformation from system coordinates to subsystem coordinates:

$$u = PU \tag{3.22}$$

where u are displacements of the subsystem degrees of freedom and U are displacements of the full system. The projection matrix in our 3-mass problem is

$$P = \begin{bmatrix} 0 & 1 & 0 \\ 0 & 0 & 1 \end{bmatrix} \tag{3.23}$$

The modal kinematics are

$$\alpha = \Psi u = \Psi P U \tag{3.24}$$

The projections of the modal forces to the full structure is

$$F = P^T f = P^T \Psi^T \psi \tag{3.25}$$

The implementation of calculation of subsystem dynamics and mapping to the full system is illustrated in Figure A.1 in Appendix A.

The calculations of the previous subsystem are repeated using the modal dissipation method. The corresponding plot for imposed load, acceleration of center mass, and relative displacements of the third and second masses are shown in Figure 3.7.

The identical agreement between the predictions of the two formulations argues strongly that they are equivalent in this instance.

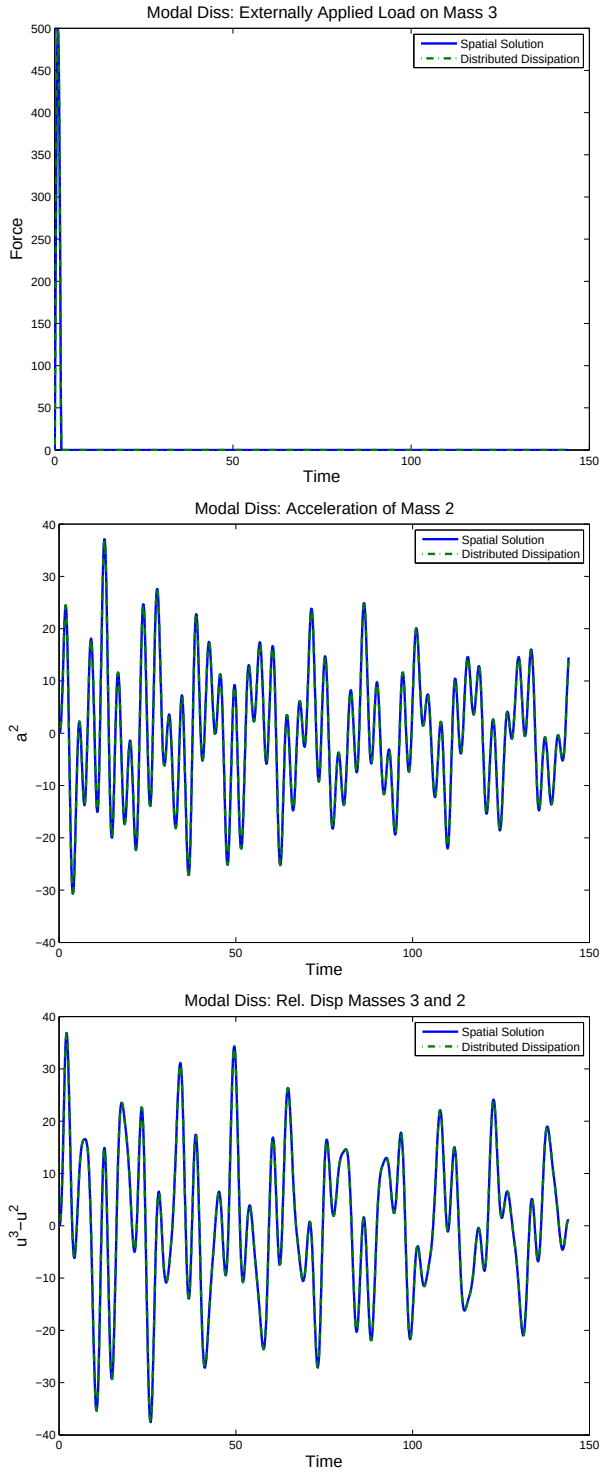

Figure 3.7. *Imposed load, acceleration of center mass, and relative displacements of the third and second masses found from numerical solution of the three-mass problem using modal dissipation for the 2-mass subsystem. The corresponding predictions from the spacial calculation are plotted also.*

Distributed Damping of the Full Three-Mass Structure

In the above section, we performed the integration of the equations of dynamics for the full system, employing a nonlinear distributed damping formulation for the subsystem and integrating that into the full system through a matrix assembly process.

In this section we employ a distributed damping formalism directly on the full system, using as primary variables the model coordinates of modes corresponding to a linearized version of the full system. Here we are not so lucky as before; we cannot derive parameters for those evolution equations in closed form. Instead, we must deduce them indirectly by examining full system response and matching parameters to that.

Again, referring to Figure 3.5, the equations of motion remain Equations 3.20 and 3.21. In the context of this problem

$$\Delta F^J = \Delta F_N (u^3 - u^2) \left\{ \begin{array}{c} 0 \\ -1 \\ 1 \end{array} \right\}. \tag{3.26}$$

The eigenfrequencies and mass-normalized eigenmodes of the linear system are $\left\{\omega^{i2},\, t^i\right\}$ We consider modal deformations $\alpha^i : i = 1:3$ and the resultant joint forces projected back onto the mode shapes.

$$\psi_i = t^{iT} \Delta F^J = \left(t_3^i - t_2^i\right) \Delta F_N \left(\alpha^i \left(t_3^i - t_2^i\right)\right) = \Delta \hat{F}_{N,i} \left(\alpha^i\right) \tag{3.27}$$

where $\hat{F}_{N,i}$ as defined in Equation 2.21.

Through a reasoning process such as used earlier, we deduce:

$$\chi_i = \chi \tag{3.28}$$

$$\beta_i = \beta \tag{3.29}$$

$$F_{Si} = \left(t_3^i - t_2^i\right) F_S \tag{3.30}$$

$$K_{Ti} = \left(t_3^i - t_2^i\right)^2 K_T \tag{3.31}$$

$$K_{\infty_i} = \left(T^T K_\infty T\right)_{i,i} \tag{3.32}$$

where $()_{i,i}$ is the i^{th} diagonal element of what is in the parentheses.

The full modal modal stiffness is

$$\omega_i^2 = K_{\infty_i} + K_{Ti} \tag{3.33}$$

Note the two major (and mathematically baseless) made implicitly above:

1. The elastic eigenvectors are preserved.
2. There is no interaction among the eigenvectors.

How well those assumptions work is explored numerically below.

A new excitation form is used:

$$F^X = \left\{ \begin{array}{c} 0 \\ 0 \\ F^{X_3} \end{array} \right\} \tag{3.34}$$

where F^{X_3} is a Morlet wavelet designed to excite the individual modes selectively.

Selective Excitation of the Third Mode

We begin with selective excitation of the third mode. (See Figure 3.8.)

This is the first example where the modal representation of distributed damping actually is an *approximation* to the truth model. Indeed we do see some small disparity between the approximate and truth models in Figure 3.9.

The distributed damping predictions look surprising good, involving what would appear to be only a modest amount of error. Examining Figure 3.10 and looking at the acceleration of the third mode - the one specifically excited by the imposed force - we again see surprisingly good agreement.

The error appears no worse when we examine the accelerations of the other two modes(Figure 3.11).

We see that for this case - where the third mode was selectively excited - the distributed dissipation model predicts the acceleration of the third modal coordinate extremely well and predicts the acceleration of the second modal coordinate just a bit less well.

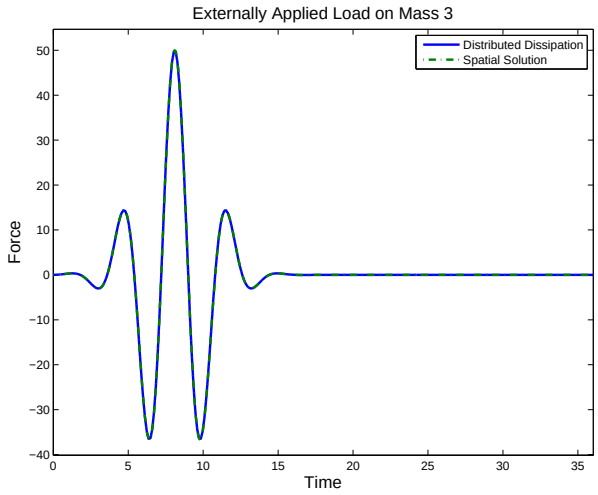

Figure 3.8. *A Morlet wavelet is employed to excite the third mode especially strongly*

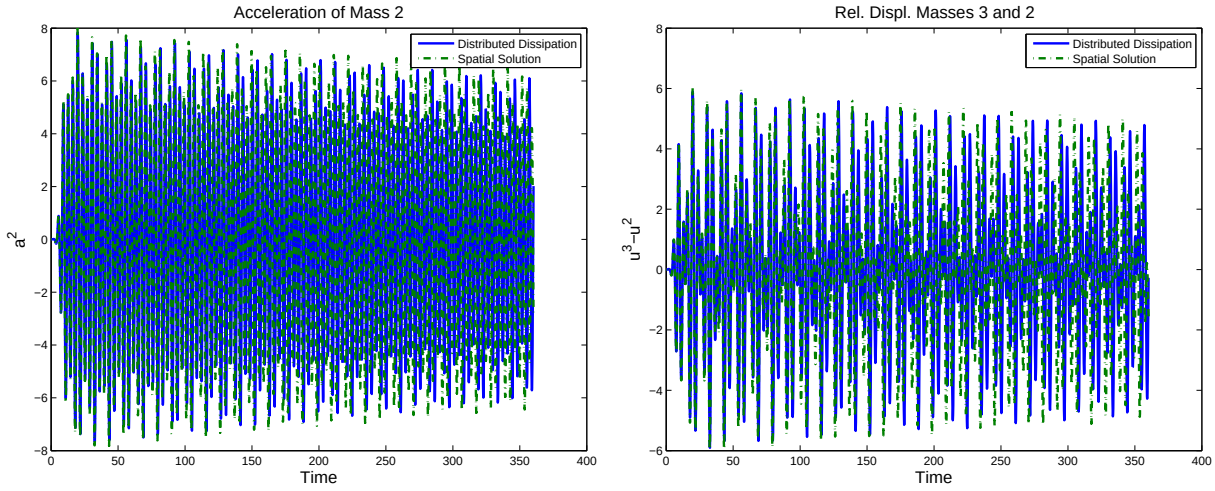

Figure 3.9. *Acceleration of center mass, and relative displacements of the third and second masses found from numerical solution of the three-mass problem using modal dissipation of full system. The corresponding predictions from the spacial calculation are plotted also.*

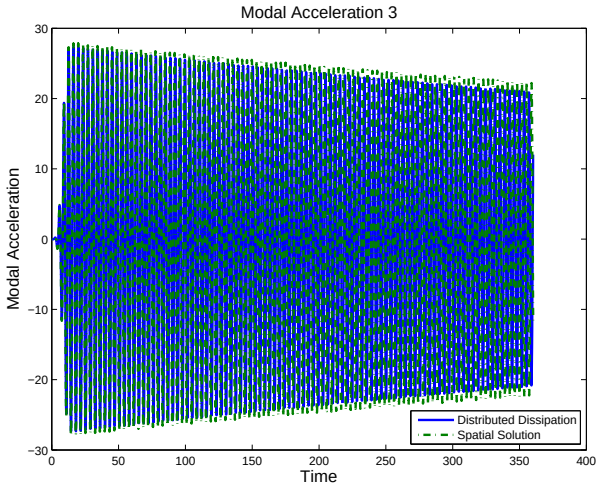

Figure 3.10. *The acceleration history of the third modal coordinate, as calculated using distributed dissipation and as calculated from a spatial solution and projected to the third mode.*

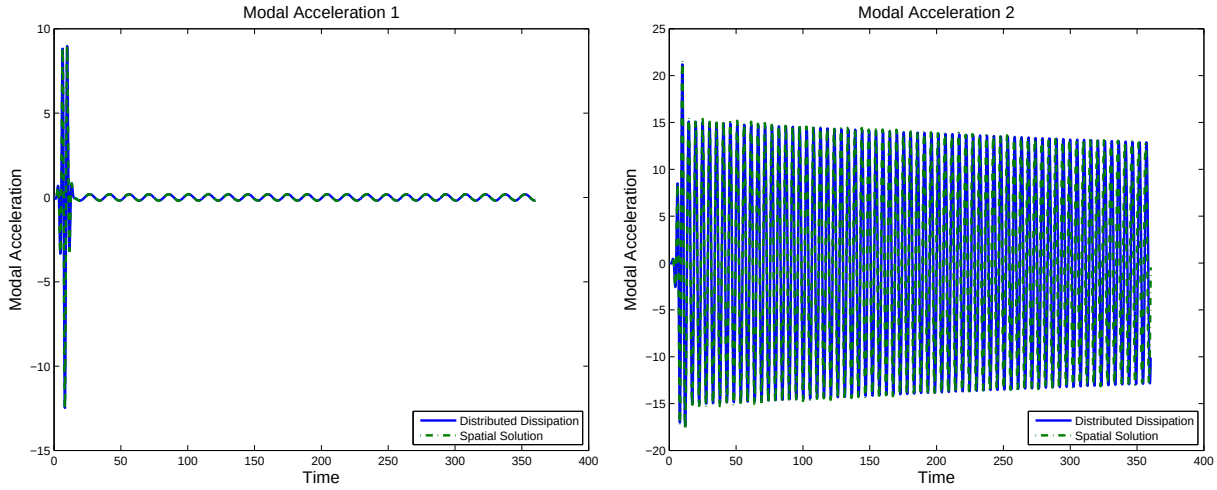

Figure 3.11. *The acceleration history of the first and second modal coordinates, as calculated using distributed dissipation and as calculated from a spatial solution and projected to those modes.*

Selective Excitation of the Second Mode

Good results occur when we selectively excite the second mode, but in Figure 3.12 we do see slightly more deviation between the predictions of the distributed dissipation model and those of the truth model. This is explored a bit more in Figure 3.13 where the second

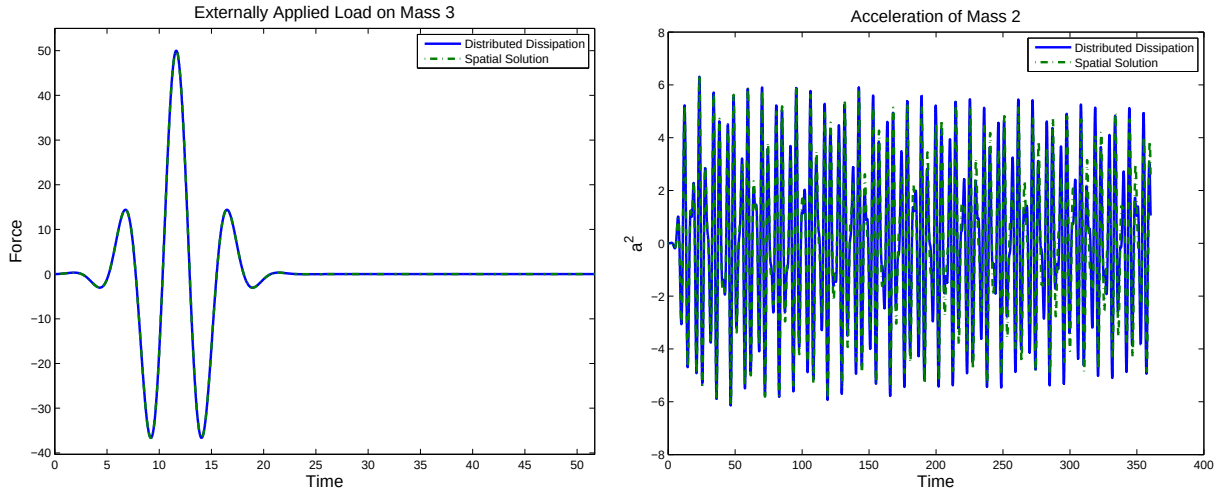

Figure 3.12. *The excitation designed to excite the second mode selectively and the resulting acceleration history of the second mass.*

and third modal accelerations are shown. (The first modal acceleration looks similar to that of the previous case.) Here we see that the second modal acceleration predicted by the distributed damping model is *very* close to that of the truth model, but there is some discernible error on the third mode.

Deducing Model Parameters from Dynamic Data

Often one is presented with an existent structure and required to predict the response of that structure to broad sets of loadings. For this one would need to calibrate a distributed damping model from a small number of experiments. Such a process on a very simple structure is discussed in this section.

First we note that under small excitations, it is generally not possible to deduce all model parameters - particularly those associated with macro-slip. On the other hand, it is what can be seen at small and modest amplitudes that needs to be captured in a model. Let's look at Iwan models capable of manifesting the dissipative behavior usually seen in jointed

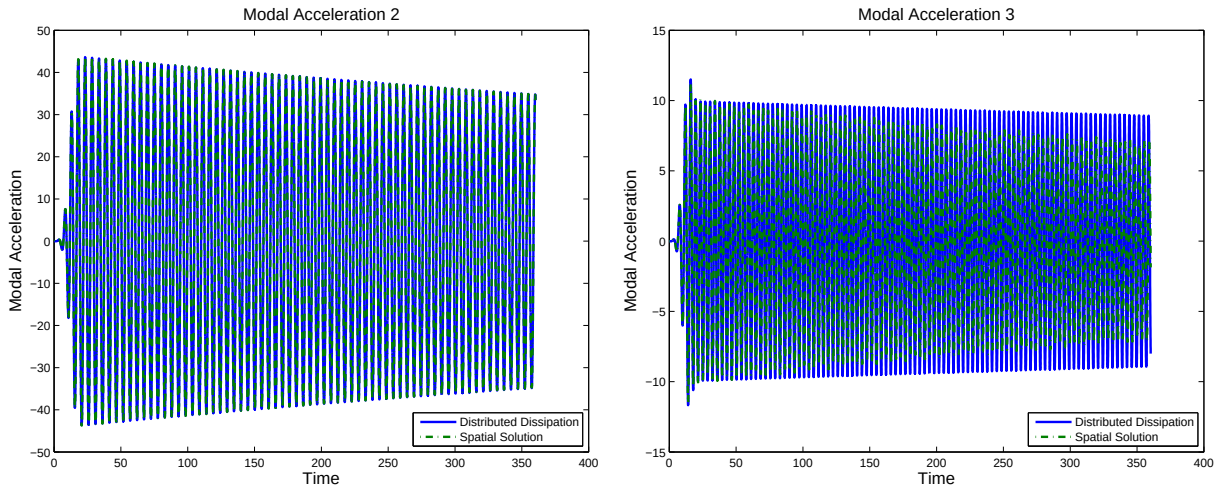

Figure 3.13. *The acceleration of the second and third modal coordinates for the case where the second mode is selectively excited.*

structures. This issue is illuminated by consideration of the class of problems considered by Palmov.

Later we discuss more intrusive experiments capable of probing for all model parameters. Both of these studies employ the the three-mass system of Figure 3.5.

Deducing Model Parameters from Small-Amplitude Harmonic Experiments

Fitting a 3-Parameter Palmov Model

Say that we have monochromatic resonance data - either harmonically driven or ring-down. At this stage, we are thinking of modal data, so the modal mass is taken as 1. From techniques such as counting zero-crossings or finding the peak of a FRF, we can deduce the stiffness:

$$K_i = \omega_i^2 \tag{3.35}$$

Also determined from those resonance experiments is energy dissipation per cycle as a function of force amplitude. In harmonic motion, Equation 3.36 yields energy dissipation in

terms of modal force ψ_i

$$D \approx C_i \, \psi^{\hat{\chi}_i+3} \tag{3.36}$$

where

$$C_i = \frac{4R_i}{K_i^{3+\hat{\chi}_i}(2+\hat{\chi}_i)(3+\hat{\chi}_i)} \tag{3.37}$$

From Equation 3.36 and the slope of the power-law dissipation we deduce $\hat{\chi}_i$. (For the specific case investigated here, Appendix B informs us that all the $\hat{\chi}_i$ are the same and are equal to the χ of the single joint in this structure.) Equations 3.36 and 3.37 can now be used to deduce R_i.

Corresponding Behavior from the 4-Parameter Model

The four-parameter Iwan model is an example of the class of constitutive model explored by Palmov and defined in Equation 1.4. With this model and the mappings from discrete joint parameters to distributed joint parameters (Equations 3.28-3.31) we have analytic expressions for the relevant small-amplitude (Palmov) joint parameters:

- K_i is determined per Equations 3.33 and 3.31.
- By Equation 3.28, $\hat{\chi}_i = \chi$ and $\hat{\beta}_i = \beta$.
- R can be expressed in terms of the four parameters as follows:

$$R_i = \frac{F_{Si}(\chi+1)}{{\phi_{\max_i}}^{\chi+2}\,(\beta+\frac{\chi+1}{\chi+2})} \tag{3.38}$$

  where

$$\phi_{\max_i} = \frac{F_{Si}(1+\beta)}{K_{Ti}\,(\beta+\frac{\chi+1}{\chi+2})} \tag{3.39}$$

An analytic expression for C_i is obtained using Equation 3.37.

A Test of Deducing Model Parameters

Just as was done in Section 3, here we ping the structure in Figure 3.5 using a short duration pulse of the sort shown in Figure 3.8 in a manner designed to excite one mode

preferentially and then use Equation 3.10 to map the global accelerations to modal accelerations. It is ring-down of those modal accelerations that is used to estimate the three relevant parameters. In fact, in the numerical experiments described here, each mode was excited at a variety of amplitudes and then permitted to ring-down for just enough cycles to obtain an estimate for stiffness and one for energy dissipation. This information was then assembled and plotted as in Figures 3 to deduce the 3 relevant parameters.

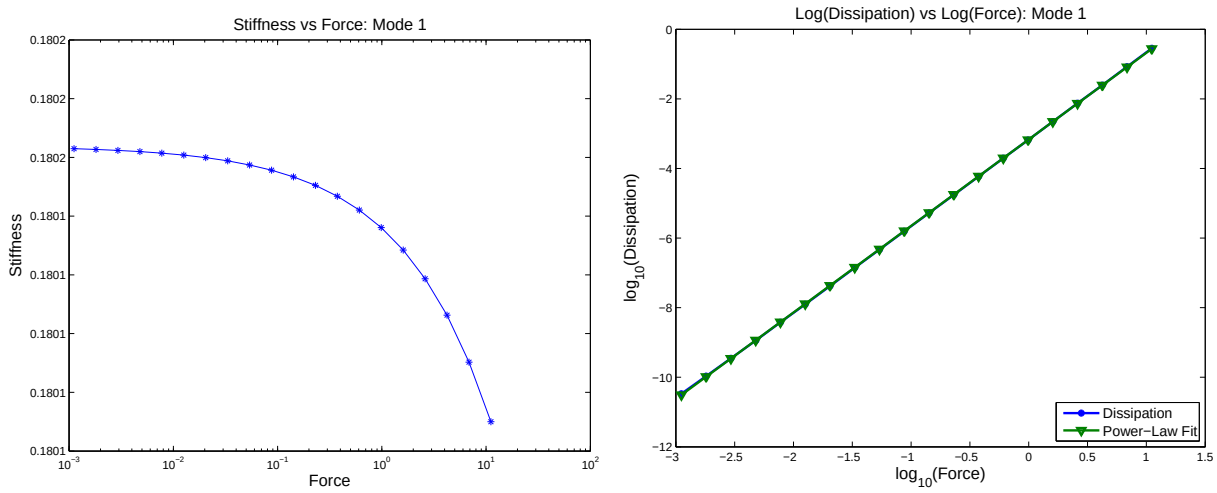

Figure 3.14. *Modal stiffness and modal energy dissipation per cycle, each as a function of modal force. Becasue the modal stiffness decreases so slowly with*

Distributed (modal) joint parameters calculated from ring-down experiments of each of the three modes, along with the analytic values, are presented in Table 3.2.

Table 3.2. Deducing Three Parameters per Mode from Ring-down Data

	Mode 1		Mode 2		Mode 3	
	Ring-Down	Analytic	Ring-Down	Analytic	Ring-Down	Analytic
$K_{0,i}$	0.18016	0.18017	1.4771	1.4779	3.0388	3.0419
χ_i	-0.50635	-0.5	-0.52957	-0.5	-0.44898	-0.5
R_i	8.91e-6	8.75e-6	9.19e-4	9.35e-4	2.88e-3	1.86e-3

We see very good agreement on modal stiffness K_i, but it is difficult to assess how close is close with respect to χ_i and R_i. For this we plot the dissipations deduced from the ring-down experiments along with those associated with the analytically derived parameters.

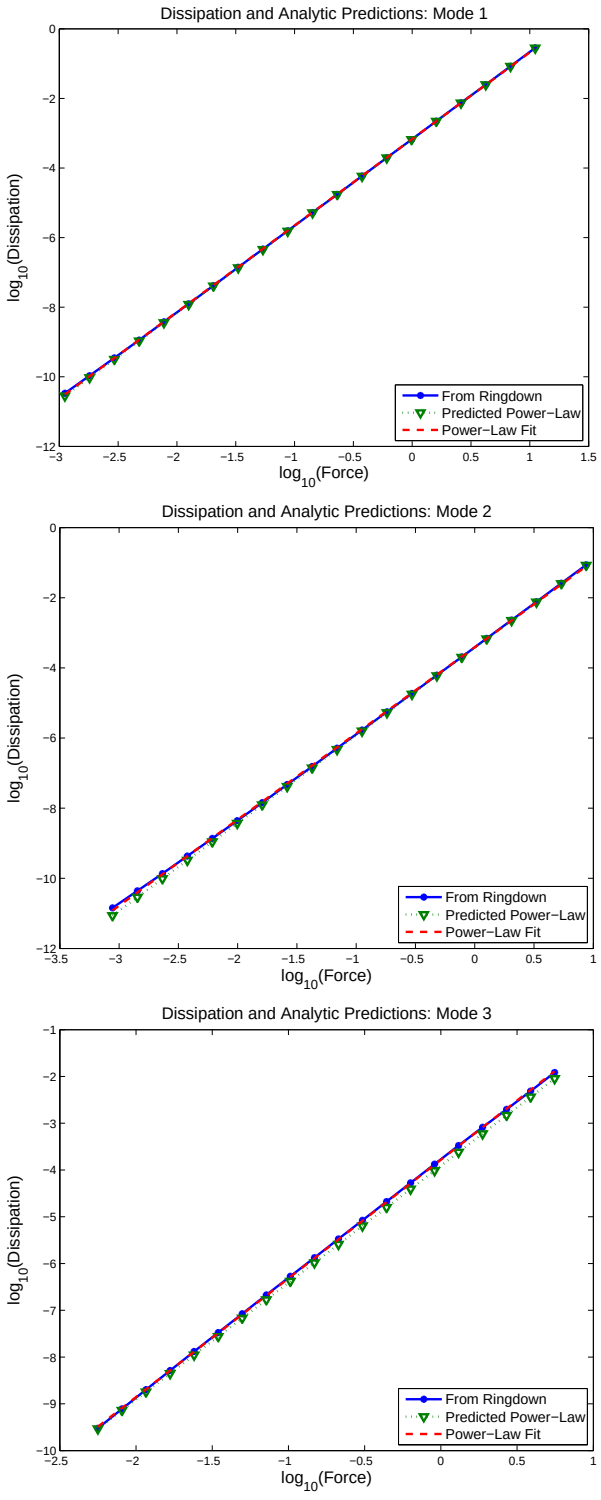

Figure 3.15. *Energy deduced from ring-down and that associated with analytic parameters.*

Overall, we see that the above process is reasonably successful in deducing correct model parameters from ring-down data. One would hope to employ this approach on experimentally obtained ring-down data with similar success.

Probing for All Parameters Using High Amplitude Excitation

Though each modal response is characterized by five parameters ($K_{\infty,m}$, $K_{T,m}$, $F_{S,m}$, χ_m, and β_m), small amplitude tests provide only three (R, χ, and K_T). We need two more "invasive" tests to obtain two more parameters. To this end, the wavelet style pinging employed in the previous section was performed at much higher amplitudes.

The results are shown in Figures 3.16 and 3.17. The stiffness versus force curve in Figure 3.16 provides one more parameter. The asymptotic behavior at small force is the $K_{0,m}$ already found from small-amplitude results. On the other hand, the asymptotic value at high force provides $K_{\infty,m}$.

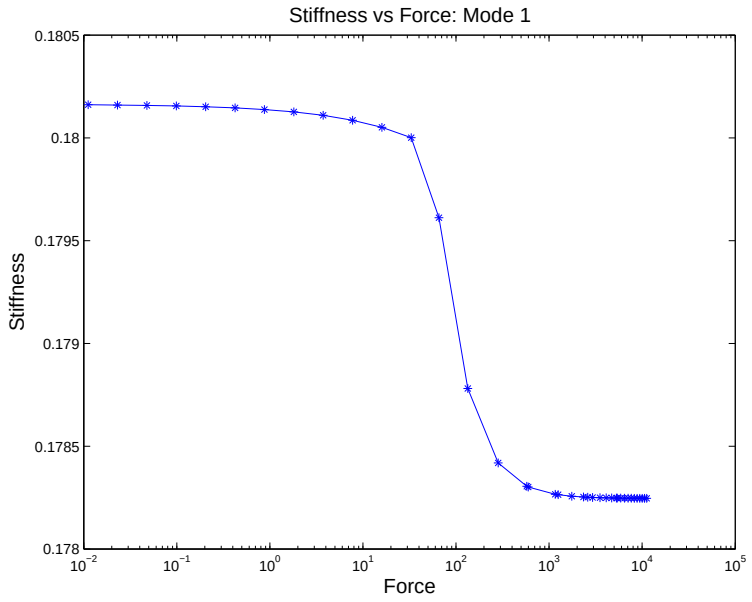

Figure 3.16. *High amplitude excitation of the structure results in softening of the modal stiffness from $K_{0,m}$ down to $K_{\infty,m}$.*

The dissipation per cycle versus force plot of Figure 3.17 also provides one more parameter. As before, the low-force data provides estimates for χ_m and R_m. The high-force asymptotic behavior provides another parameter. We note that in the regime of very high amplitude oscillation, the dissipation per cycle will be $4UF_{S,m}$ where U is the amplitude of oscillation. In this one dimensional system $U = F/\omega^2$, so F_S can be deduced from a linear fit to the log-log behavior of dissipation at large loads.

We now have five parameters ($K_{0,m}$, $K_{\infty,m}$, $F_{S,m}$, χ_m, and R_m) from which we can solve for the canonical parameters ($K_{T,m}$, $K_{\infty,m}$, $F_{S,m}$, χ_m, and β_m). The solution process is as follows:

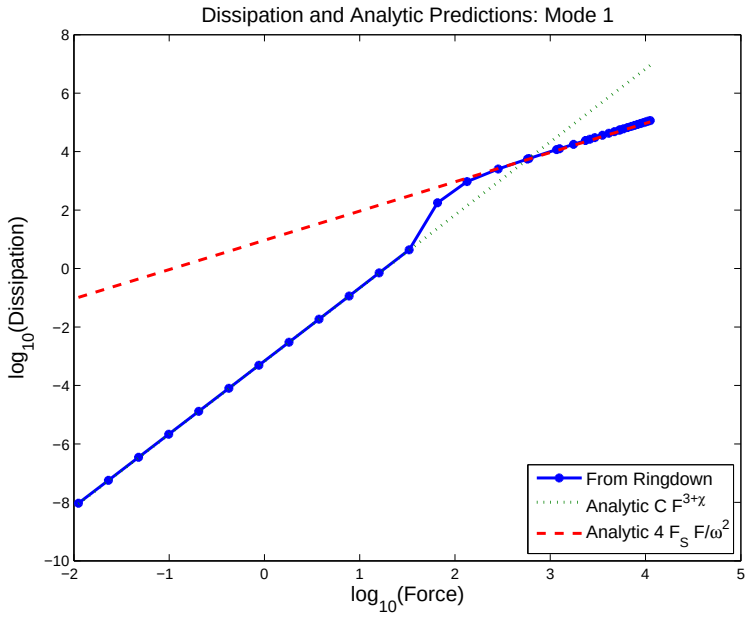

Figure 3.17. *Response to high amplitude excitation of the structure shows two distinct power-law regimes of dissipation: one associated with micro-slip and one associated with macro-slip.*

1. $K_{\infty,m} = K_{\infty,m}$
2. $F_{S,m} = F_{S,m}$
3. $\chi_m = \chi_m$
4. $K_{T,m} = K_{0,m} - K_{\infty,m}$
5. Equations 25 and 27 of [27] are solved numerically for β in favor of R.

Table 3.3. Deducing Five Parameters per Mode from Ring-down Data

	Mode 1		Mode 2		Mode 3	
	Ring-Down	Analytic	Ring-Down	Analytic	Ring-Down	Analytic
$K_{T,i}$	0.0019146	0.0017271	0.079049	0.072533	0.11052	0.12574
$K_{\infty,i}$	0.17825	0.17845	1.398	1.4054	2.9283	2.9162
$F_{S,i}$	0.4605	0.41559	2.7711	2.6932	4.8469	3.546
χ_i	-0.50635	-0.5	-0.52957	-0.5	-0.44898	-0.5
β_i	5.7329	5	6.2431	5	1.1706	5

Conclusions

1. In the one case that I have found for which the distributed damping is an exact model for the subsystem (the two mass system), the distributed dissipation model matches the truth (spatial) model exactly.

2. For the case of a three mass system, the assumptions of modal independence are truly only a coarse *approximation* to reality. In this case, overall predictions of acceleration are pretty good, but there are some errors in detail.

3. The limited sets of simulations explored here suggest that the distributed damping approximation predicts best the accelerations of modal coordinates corresponding to the strongest excitation frequencies.

4. The modally distributed damping formalism provides the potential for massive improvements in computational efficiency, but whether this approach remains stable for large systems will require some experimentation.

5. The derivation presented here, as well as the code written to explore it, manifest many opportunities for sign errors. Let's be careful about this.

References

[1] J Bauschinger. Über die Veränderung der Elastizitätsgrenze und der Festigkeit des Eisens und Stahls durch Strecken und Quetschen, durch Erwärmen und Abkühlen und durch oft mal wiederholte Beanspruchung. (on the change in elastic limit and strength of iron and steel in tension and compression through heating and cooling and cyclic stress). Technical Report vol. 13, n. 1., Mechanisch-technischen Laboratorium der Königlichen Technischen Hochschule, Munich, 1886.

[2] Manoj Bhardwaj, Kendall Pierson, Garth Reese, Tim Walsh, David Day, Ken Alvin, James Peery, Charbel Farhat, and Michel Lesoinne. Salinas: A scalable software for high-performance structural and solid mechanics simulations. *SC Conference*, 0:35, 2002.

[3] D. Y. Chiang. The generalized masing model for deteriorating hysteresis and cyclic plasticity. *Applied Mathematical Modeling*, 23:847–863, 1999.

[4] Nikolai Nikolaevich Davidenkov. On energy dissipation in vibrations. *Journal of Technical Physics*, 8(6):483, 1938.

[5] Danny L. Gregory, Ronald Coleman, and David O. Smallwood. Applications of a six-DOF electrodynamic shaker system for finite element model validation and component testing. In *Proceedings of the 80th Shock and Vibration Symposium, San Diego*, October 2009.

[6] Danny Lynn Gregory, David Ora Smallwood, and Ronald G. Coleman. Experimental studies to investigate damping in frictional shear joints. In *Proceedings of the 70th Shock and Vibration Symposium, held Nov 1999 in Albuquerque, NM,*. Shock and Vibration Information Analysis Center, Arvonia, VA 23004, 1999. SAND99-2255A.

[7] Akira Harada, Yukinori Kobayashi, and Gen Yamada. Reduced-order nonlinear modal equations of plates based on the finite element method. *JSME International Journal Series C*, 45:79–86, 2002.

[8] Martin W. Heinstein and Daniel J. Segalman. Bending effects in the frictional energy dissipation in lap joints. Technical Report SAND2002-0083, Sandia National Laboratories, PO Box 5800, Albuquerque, NM 87185, January 2002.

[9] A. Yu. Ishlinskii. Some applications of statistical methods to describing deformations of bodies. *Izvestiya Akademii Nauk SSSR*, 9:580–590, 1944.

[10] W. D. Iwan. Distributed-element model for hysteresis and its steady-state dynamic response. *ASME Journal of Applied Mechanics*, 33(4):893–900, Dec. 1966.

[11] W. D. Iwan. On a class of models for yielding behavior of continuous and composite systems. *ASME Journal of Applied Mechanics*, 34(3):612–617, 1967.

[12] Marie B. Levine and Christopher White. Microdynamic analysis for establishing nanometric stability requirements of jointed precision space structures. *Proceedings of the International Modal Analysis Conference, Paper No. 325, Kissimmee Fl.*, Feb 2001.

[13] Hermann G. Matthies and Marcus Meyer. Nonlinear Galerkin methods for the model reduction of nonlinear dynamical systems. *Computers and Structures*, 81:12771286, 2003.

[14] Zenon Mröz. On the description of anisotropic workhardening. *J. Mech. Phys. Solids*, 15:163–175, 1967.

[15] Arlene Ann O'Sean, Antoinette Tingley Schleyer, and Ellen Swanson. *Mathematics into Type*. American Mathematical Society, Providence, RI, 1999.

[16] Vladimir Palmov. *Vibrations of Elasto-Plastic Bodies*. Springer, 1998. "Translated by A. Belyaev".

[17] C.-Y. Peng. *Generalized Model Identification of Linear and Nonlinear Dynamic Systems*. PhD thesis, California Institute of Technology, 1988.

[18] L. Prandtl. Ein gedankenmodell zur kinetischen theorie der festen körper. *Z. Angew. Math. Mech. (ZAMM)*, 8:85–106, 1928.

[19] Garth M. Reese, Manoj Kumar Bhardwaj, Daniel Joseph Segalman, Kenneth Fredrick Alvin, and Brian James Driessen. Salinas user's notes. Technical Report SAND99-2801, Sandia National Laboratories, PO Box 5800, Albuquerque, NM, November 1999.

[20] Daniel J. Segalman. Modelling joint friction in structural dynamics. *Structural Control and Health Monitoring*, 13(1):430–453, 2005.

[21] Daniel J. Segalman. Model reduction of systems with localized nonlinearities. *Journal of Computational and Nonlinear Dynamics*, 2(3):249–266, July 2007.

[22] Daniel J. Segalman, Lawrence A. Bergman, and David J. Ewins. Report on the SNL/NSF International Workshop on Joint Mechanics Arlington Virginia, 16-18 October 2006. Technical Report SAND2007-7761, Sandia National Laboratories, Albuquerque, New Mexico 87185, January 2008.

[23] Daniel J. Segalman, Danny L. Gregory, Michael J. Starr, Brian R. Resor, Michael D. Jew, James P. Lauffer, and Nicoli M. Ames. Handbook on dynamics of jointed structures. Technical Report SAND2009-4164, Sandia National Laboratories, Albuquerque, New Mexico 87185 and Livermore, California 94550, July 2009.

[24] Daniel J. Segalman and Wil Holzmann. Nonlinear response of a lap-type joint using a whole-interface model. *Proceedings of the 23rd International Modal Analysis Conference (IMAC-XXIII), held in Orlando, Florida, USA*, Feb. 2005.

[25] Daniel J. Segalman and Michael J. Starr. Inversion of Masing models via continuous Iwan systems. *International Journal of Non-Linear Mechanics*, 43:74–80, 2008.

[26] Daniel Joseph Segalman. An initial overview of Iwan modeling for mechanical joints. Technical Report SAND2001-0811, Sandia National Laboratories, 2001.

[27] Daniel Joseph Segalman. A four-parameter Iwan model for lap-type joints. *ASME Journal of Applied Mechanics*, 72(5):752–760, September 2005.

[28] Daniel Joseph Segalman and Michael James Starr. Relationships among certain joint constitutive models. Technical Report SAND2004-4321, Sandia National Laboratories, PO Box 5800, Albuquerque, NM, September 2004.

[29] D. O. Smallwood, D.L. Gregory, and R. G. Coleman. A three-parameter constitutive model for a joint which exhibits a power law relationship between energy loss and relative displacement. *Proceedings of the 72nd Shock and Vibration Symposium, Destin, FL*, Nov 2001. Available form SAVIAC.

[30] E. E. Ungar. Energy dissipation at structural joints: Mechanisms and magnitudes. Technical Report FDL-TDR-64-98, US Air Force Flight Dynamics Laboratory, 1964.

[31] E. E. Ungar. Damping in built-up structures. *Journal Of The Acoustical Society Of America*, 45(1):319, 1969.

[32] E. E. Ungar. The status of engineering knowledge concerning the damping of built-up structures. *Journal of Sound and Vibration*, 26(1):141 – 154, 1973.

Appendix A

Illustration of Integration of Subsystem Dynamics into Full-System Dynamics

The implementation of calculation of subsystem dynamics and mapping to full system is illustrated in Figure A.1.

```
 1 % this is a null version of the states function for a single degree of
 2 % freedom system
 3 function [Fx, states, Kx] = Modal_3Mass_Joint_Force(D, states,↙
ModelParams)
 4 global  ommega gammma;
 5 % find joint properties
 6
 7 % map global displacement vector to local displacement vector
 8 P =[0 1 0; 0 0 1];
 9 DL = P*D;
10
11 % map local displacement to relevant modal coordinate
12 T=gammma*[1 -1; 1 1];  % T maps modal displacements to local
13 R = T^(-1);            % R maps local displacements to modal
14 alpha = R*DL;
15
16
17 % Calculate modal force and stiffness associated with that
18 %  second mode. (We know that the first mode is a rigid body
19 %  motion and contributes no joint forces.)
20 % Note that following code exploits exact understanding
21 %  of source of modal damping for this problem
22 [FJ, states, KJ]=iwan_NewParams(alpha(2) ,states, ModelParams);
23 K_T  = ModelParams(3);
24 F_elast= K_T*alpha(2);
25 phi =  [0; (F_elast-FJ)];
26 grad = (K_T-KJ)*[0 0; 0 1];
27
28 % Convert from Modal Forces to Forces in Local Frame
29 FxL   = R'*phi;
30 gradL = R'*grad*R;
31
32 % convert from local Forces and Gradient to global
33 Fx = P'*FxL;
34 Kx = P'*gradL*P;
35
36
```

Figure A.1. *Matlab code calculating subsystem distributed damping and mapping it to the full system coordinates.*

Appendix B

Derivation of Modal BPII Distribution Function from Joint BPII Distribution Functions

Among the directions identified in an 2003 LDRD proposal on model reduction by the author was

> *"Develop Mathematical Formulation: The first approach to be explored is that of devising a modal expression for the nonlinear dynamics of jointed structures (or structures of similar nonlinearity) using the eigenmodes of a corresponding linear structure combined in a nonlinear manner. This will involve using modal participation factors in the vicinities of the joints along with Hamilton's principle to derive nonlinear evolution equations for modal coefficients."*

Despite the small mis-wording ("modal participation factors" should have been "modal displacements") the above paragraph captures well the thrust of the research presented in this document.

Though that proposal did get funded, the particular research thrust identified in that paragraph was set aside in order to pursue another interesting model reduction approach [21]. The work presented in the body of this document facilitates the derivation suggested in that 2003 proposal and that derivation is presented here.

Using the notion introduced in the body of this document, consider a jointed structure having

- Mass matrix M.
- Linearized stiffness matrix K^0.
- Stiffness matrix K^∞ if the joints are replaced by gaps.
- Eigenvectors $\{\Phi_k\}$ of system (M, K^0). The full displacement field is represented

$$u(t) = \sum_k \alpha^k \Phi_k \tag{B.1}$$

It is assumed that these eigenvectors are orthonormal with respect to matrix M. The corresponding eigenvalues are ω_k^2.

- $\Delta\Phi_{k,j}$ the gap across the j^{th} joint associated with the k^{th} mode. In general each $\Delta\Phi_{k,j}$ is a 3-vector representing either rotations or displacements. We represent $\Delta\Phi_{k,j}$ as

$$\Delta\Phi_{k,j} = s_{k,j} v_j \tag{B.2}$$

where $s_{k,j}$ is a scalar and v_j is a unit vector: $v_j^T v_j = 1$. The gap across the j^{th} joint is now

$$\Delta u_j(t) = \sum_k \alpha^k s_{k,j} v_j \tag{B.3}$$

The Euler equations associated with Hamilton's principle are the Lagrange equations and these are employed in the following to derive the equations of motion associated with each modal coordinate. We consider one modal coordinate at a time.

The kinetic energy is

$$T = \dot{\alpha}_k^2/2 \tag{B.4}$$

Exclusive of the strain energy in the joints, the potential energy is

$$V^\infty = \alpha_k^2 \ \Phi_k^T K^\infty \Phi_k \tag{B.5}$$

The generalized forces are those due to the physical forces that the joints apply to the rest of the structure:

$$Q_k = -\sum_j \left(\int_0^\infty \left[\alpha^k s_{k,j} - x_{k,j}(t,\phi) \right] \ \rho_j(\phi)\, d\phi\, v_j^T \right) (s_{k,j} v_j) \tag{B.6}$$

where ρ_j is the BPII distribution function for the j^{th} joint and $x_{k,j}$ evolves as

$$\dot{x}_{k,j}(t,\phi) = \begin{cases} \dot{\alpha}\, s_{k,j} & \text{if } \|\alpha\, s_{k,j} - x_{k,j}(t,\phi)\| = \phi \text{ and } \dot{\alpha^k}(\alpha^k s_{k,j} - x_{k,j}(t,\phi)) > 0 \\ 0 & \text{otherwise} \end{cases} \tag{B.7}$$

Recalling Equation 2.22, repeated here,

$$\dot{\beta}_k(t,\phi) = \begin{cases} \dot{\alpha}_k & \text{where} \quad \dot{\alpha}_k \left(\alpha^k - \beta^k \right) > 0 \quad \text{and} \quad \left| \alpha^k - \beta^k \right| = \phi \\ 0 & \text{otherwise} \end{cases}$$

we see that

$$x_{k,j}(t,\phi) = s_{k,j}\,\beta^k(t,\phi/s_{k,j}) \tag{B.8}$$

for all j.

Equation B.6 now becomes

$$Q_k = -\sum_j s_{k,j}^2 \int_0^\infty \left[\alpha^k - \beta^k(t,\phi/s_{k,j})\right] \rho_j(\phi) d\phi \tag{B.9}$$

Defining

$$L = T - V^\infty \tag{B.10}$$

our equation of motion is

$$\frac{\partial L}{\partial \alpha^k} - \frac{d}{dt}\frac{\partial L}{\partial \dot{\alpha}_k} = Q_k \tag{B.11}$$

$$\ddot{\alpha}_k + \left(\Phi_k^T K^\infty \Phi_k + \sum_j s_{k,j}^2 \int_0^\infty \rho_j(\phi) d\phi\right) \alpha^k = \sum_j s_{k,j}^3 \int_0^\infty \beta^k(t,\acute{\phi})\,\rho_j(s_{k,j}\acute{\phi}) d\acute{\phi} \tag{B.12}$$

Since for small loads the right hand side of Equation B.12 goes to zero, the left hand side must be the equation of motion for the linearized system:

$$\omega_k^2 = \Phi_k^T K^\infty \Phi_k + \sum_j s_{k,j}^2 \int_0^\infty \rho_j(\phi) d\phi \tag{B.13}$$

Examination of the right hand side of Equation B.12 provides us an expression for the BPII distribution function for mode k

$$\rho_k^{\text{modal}}(\phi) = \sum_j s_{k,j}^3\,\rho_j(s_{k,j}\phi) \tag{B.14}$$

which defines the constitutive behavior of each mode.

Appendix C

Calculation of State Variables

Calculation of joint forces (and of generalized forces, in the case of distributed damping) is one of the more formidable issues in using BPII models. Following, some useful closed-form and approximate expressions are derived for the case where the joint (or generalized) displacement is driven harmonically.

The generalized force has the form

$$\Delta\mathcal{Q}_j = \int_0^\infty x_j(t,\phi)\,\rho_j(\phi)\,d\phi \tag{C.1}$$

where $x_j(t,\phi)$ evolves as

$$\dot{x}_j(t,\phi) = \begin{cases} \dot{u} & \text{if } \|u(t) - x_j(t,\phi)\| = \phi \text{ and } \dot{u}(u - x_j(t,\phi)) > 0 \\ 0 & \text{otherwise} \end{cases} \tag{C.2}$$

and u is the joint (or generalized) displacement.

Performing the relevant integrations to evaluate $\Delta\mathcal{Q}_j$ is facilitated by some observations that can be obtained by scrutiny of Figure C.1. Shown in that figure are cyclic displacements $u(t) = A\sin(t)$ and the $x(\phi,t)$ that evolve as in Equation C.2.

This figure suggests the following explicit expressions for x

$$\begin{aligned} &\text{for } \dot{u} > 0 \\ &\qquad x = \begin{cases} u - \phi & \text{for} \quad 0 < \phi < (u + A)/2 \\ -A + \phi & \text{for} \quad (u + A)/2 < \phi < A \end{cases} \\ &\text{for } \dot{u} < 0 \\ &\qquad x = \begin{cases} u + \phi & \text{for} \quad 0 < \phi < (A - u)/2 \\ A - \phi & \text{for} \quad (A - u)/2 < \phi < A \end{cases} \end{aligned} \tag{C.3}$$

The next step in the evaluation of $\Delta\mathcal{Q}_k$ is the evaluation of the the integral in Equation C.1 and, for reasons discussed in the body of this monograph, we employ the Palmov distribution (Equation 1.4)

$$\mathcal{Q}(u) = \int_0^\infty x(t,\phi)\rho(\phi)d\phi = \int_0^A x(t,\phi)R\phi^\chi\,d\phi \tag{C.4}$$

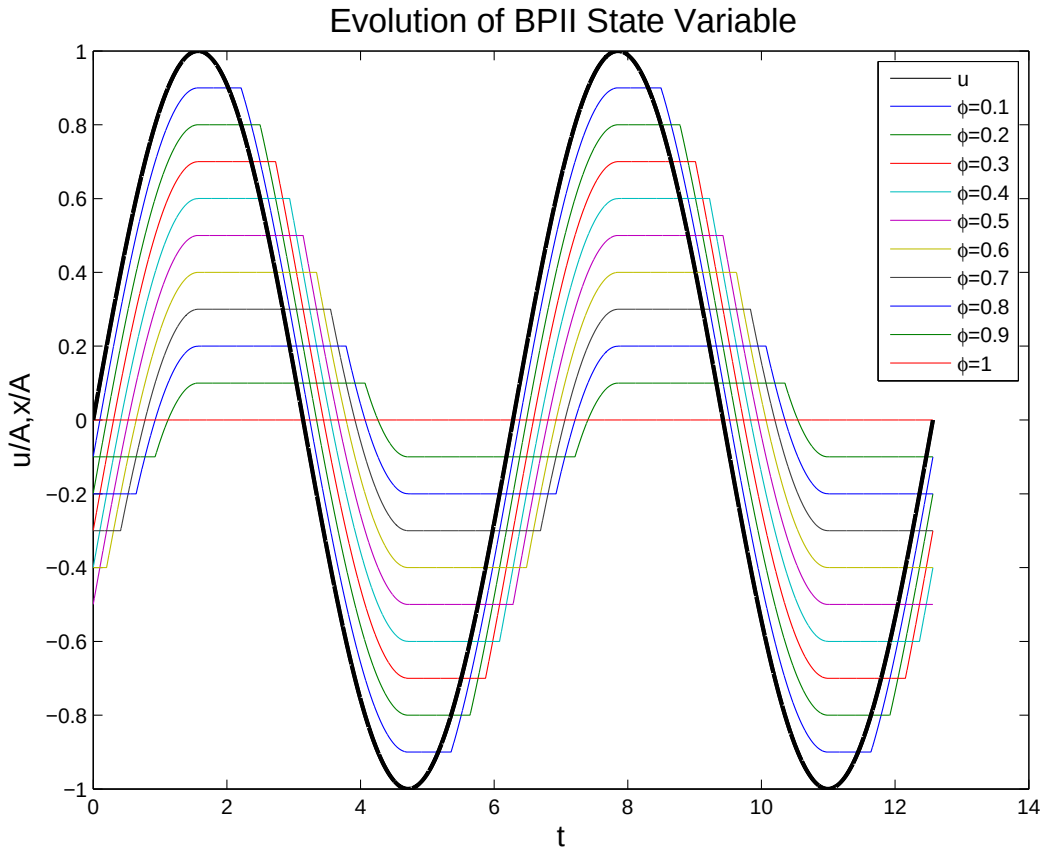

Figure C.1. *The evolution of state variable $x(\phi, t)$ under harmonic loading.*

where A is the amplitude of displacement $u(t)$. The range of integration is shortened because $\|x\| < A$ for all ϕ and all u.

We find for $\dot{u} > 0$

$$\Delta\mathcal{Q}(u) = R\frac{\left((u+A)^{\chi+2}\,2^{-(\chi+1)} - A^{\chi+2}\right)}{(\chi+1)\,(\chi+2)} \tag{C.5}$$

For $\dot{u} < 0$,

$$\Delta\mathcal{Q}(u) = -R\frac{\left((A-u)^{\chi+2}\,2^{-(\chi+1)} - A^{\chi+2}\right)}{(\chi+1)\,(\chi+2)} \tag{C.6}$$

We may use the above to plot $\Delta\mathcal{Q}(u)$ and u vs time for different amplitudes A (Fig C.2). We see that the modal force is roughly sinusoidal with the period of the imposed displacement u.

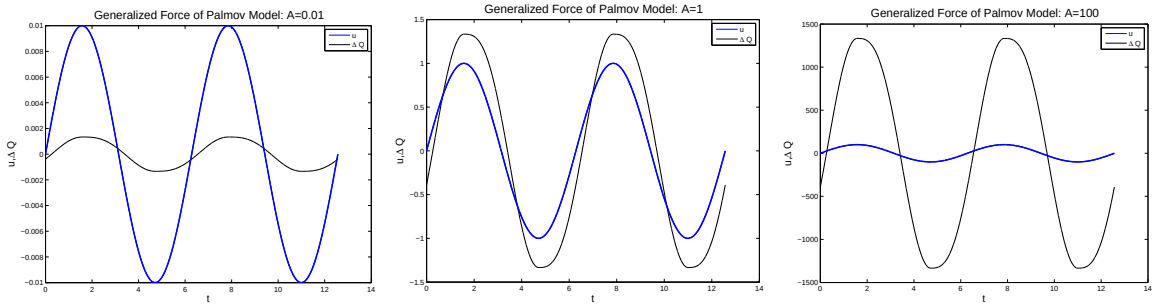

Figure C.2. *The modal force over two cycles for several amplitudes of displacement.*

Letting $u(t) = A\sin(t)$, the generalized force is approximated by

$$\Delta\mathcal{Q} \approx R\,\left[C_1(A)\sin(t) + C_2(A)\cos(t)\right] \tag{C.7}$$

Performing the relevant evaluation of Equations C.5 and C.6 for multiple values of A we perform the appropriate least-squares fit to obtain $C_1(A)$ and $C_2(A)$. Defining

$$B(A) = \sqrt{C_1^2 + C_2^2} \quad \text{and} \quad \gamma(A) = \tan^{-1}(C_2/C_1) \tag{C.8}$$

we now plot each of $B(A)$ and $\gamma(A)$ vs A in Figure C.3. In the problem presented here, parameters R and χ were specified as $R = 1$ and $\chi = -1/2$.

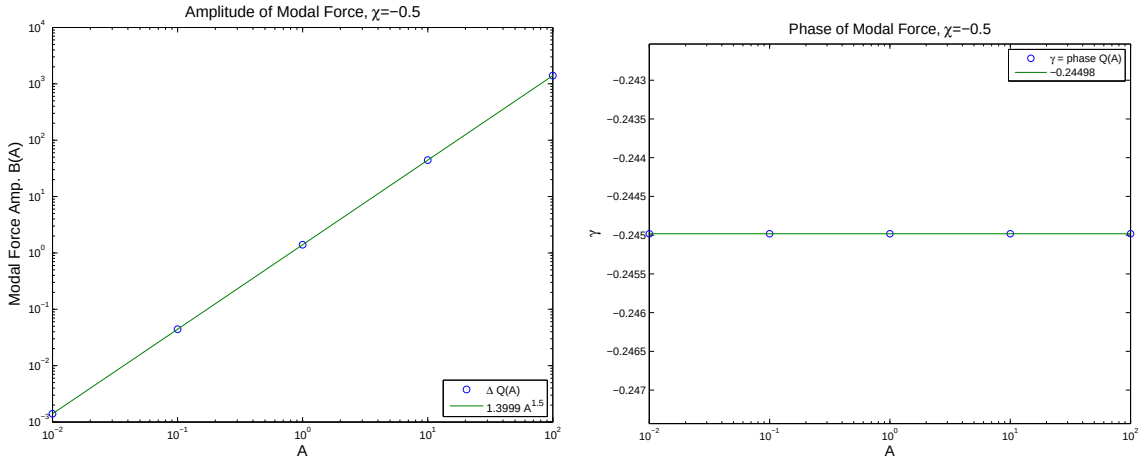

Figure C.3. *The amplitude and phase of modal force as functions of imposed displacement.*

On the basis of that figure, we express

$$B(A) = 1.4\,A^{3/2} \quad \text{and} \quad \gamma(A) = -0.245 \tag{C.9}$$

The modal force is now expressed

$$\Delta\mathcal{Q}(A) = R\,B(A)\,[\cos(\gamma)\sin(t) + \sin(\gamma)\cos(t)] = R\,B(A)\sin(t+\gamma) \tag{C.10}$$

where, for the case of $\chi = -0.5$, $B(A)$ and $\gamma(A)$ are as given in Equation C.9.

In fact, if we perform the similar calculations for an array of values for χ, we observe that the relations found in the above case hold for general χ. Letting

$$B(A, \chi) = C(\chi)A^{\theta(\chi)} \tag{C.11}$$

where $C(\chi)$ and $\theta(\chi)$ are shown graphically in Figure C.4

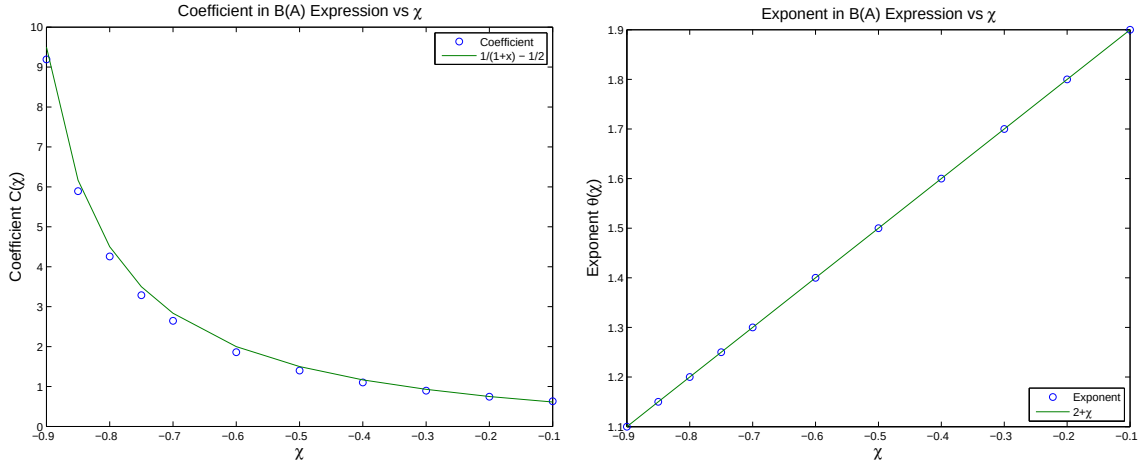

Figure C.4. *Coefficient $C(\chi)$ and exponent $\theta(\chi)$ used in Equation C.11.*

We see that $C(\chi)$ can be approximated reasonably well by

$$C(\chi) \approx \frac{1}{1+\chi} - \frac{1}{2} \tag{C.12}$$

and that $\theta(\chi)$ can be approximated with great precision by

$$\theta(\chi) = 2 + \chi \tag{C.13}$$

This last equation should not be too surprising since $\Delta\mathcal{Q}$ is a dissipative force and $u \sim A$ is a displacement, so dissipation goes as $u\,\Delta\mathcal{Q} \sim A^{3+\chi}$, which is true by construction.

As was illustrated in the case of $\chi = -0.5$, the phase shift γ remains independent of A for other values of χ as well. The dependence of γ on χ is shown in Figure C.5.

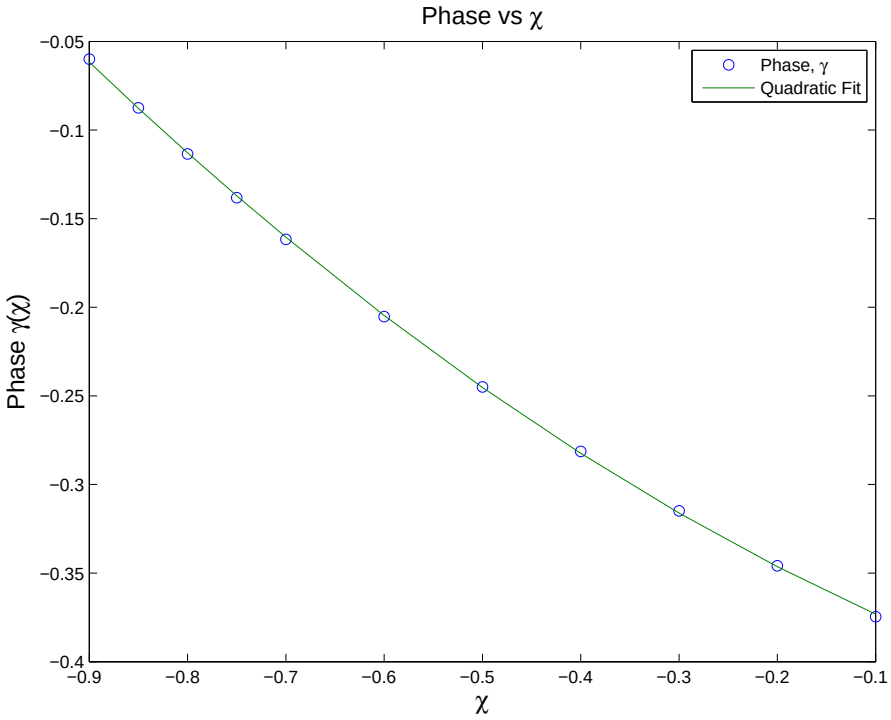

Figure C.5. *The phase difference between harmonic displacement of joint and the resulting joint force.*

In that figure, we see that the phase shift can be represented extremely well by a quadratic approximation:

$$\gamma(\chi) \approx P(\chi) = 0.1738\chi^2 - 0.2155\chi - 0.3965 \tag{C.14}$$

We may now assert that for general χ the generalized force associated with harmonically driven generalized displacements is represented adequately by Equation C.10 where $B(A)$ is evaluated using Equations C.11 and Equations C.12 and C.13 and $\gamma(\chi)$ is approximated by Equation C.14.

DISTRIBUTION:

5 Professor David Ewins
University of Bristol
Queen's Building
University Walk
Clifton, Bristol BS8 1TR
London
England

5 Professor Lawrence Bergman
306 Talbot Lab
104 S. Wright St.
University of Illinois
Urbana, IL 61801

1 Professor Edward Berger,
Department of Civil Engineering
The University of Virginia
Thornton Hall, Office: D203
351 McCormick Road
PO Box 400742
Charlottesville, VA 22904-4742

1 Daniele Dini
Imperial College London,
South Kensington Campus,
London
SW7 2AZ
UK

1 Greg Garay,
Leader, Damping Technology
GE Aircraft Engines
One Neumann Way MD-A413
Cincinnati, OH 45215

1 Kevin Garraway
Engineering Analysis Group
AWE Aldermaston
Reading
RG7 4PR
England, UK

1 Lothar Gaul
Institut A für Mechanik
Universität Stuttgart
Pfaffenwaldring 9
Zimmer 3.127
Stuttgart 70550
Germany

1 Dr. Jennifer Gresham,
Air Force Office of Scientific Research
875 North Randolph Street, Suite 325
Arlington, VA 22203

1 Professor David Hills,
Department of Engineering Science
University of Oxford
Oxford, OX1 3PJ
England, UK

1 Professor Tod A. Laursen,
127 Hudson Hall
Box 90287
Duke University
Durham, NC 27708

1 Professor Arif Masud
Department of Civil & Environmental Engineering,
University of Illinois at Urbana-Champaign
Urbana, IL 61801

1 Dr. Eduardo Misawa,
The National Science Foundation,
4201 Wilson Boulevard,
Arlington, Virginia 22230

1 Dr. Evgeny Petrov,
Mechanical Engineering Department
Imperial College London
South Kensington Campus
London, SW7 2AZ,
UK

1 Professor Dane Quinn
Dept. of Mechanical Engineering
The University of Akron
Akron, OH 44325-3903

1 Dr. Lawrence Robertson
U.S. Air Force Research Laboratory
AFRL/VSSV
3550 Aberdeen Avenue SE
Kirtland AFB, NM 87117

1 Surya Surampudi
EOARD
86 Blenheim Crescent
Hillingdon, Ruislip, Greater London
England
HA4 7HB
UK

1 Alexander Vakakis
3003 Mechanical Engineering Laboratory
1206 West Green Street, MC-244
Urbana, IL 61801

1 Professor David Wang-Kerr
Texas A&M University
Department of Mechanical Engineering
3123 TAMU
College Station TX 77843-3123

1 MS 0110 Justine E. Johannes, 01220
1 MS 0346 Michael J. Starr, 01526
1 MS 0346 Michael A. Guthrie, 01523
1 MS 0346 Thomas Baca, 01523
1 MS 0346 Michael Ross, 01523
1 MS 0346 Jerry W. Rouse, 01523
1 MS 0346 D. Gregory Tipton, 01523
1 MS 0372 Huei Eliot Fang, 01524
1 MS 0372 James M. Redmond, 01525
1 MS 0380 David Womble, 01540
1 MS 0380 Joseph Jung, 01542
1 MS 0380 Garth M. Reese, 01542
1 MS 0384 Duane B. Dimos, 01500
1 MS 0431 John Pott, 00511
1 MS 0557 Todd W. Simmermacher, 01523
1 MS 0557 Christian C. O'Gorman, 01522
1 MS 0557 Danny L. Gregory, 01521
1 MS 0557 Randall L. Mayes, 01522
1 MS 0557 Sarah Leming, 01521

1	MS 0557	Darrick M. Jones, 01521
1	MS 0557	Fernando Bitsie, 01521
1	MS 0557	Eric C. Stasiunas, 01521
1	MS 0834	Mikhail Mesh, 01523
1	MS 0847	Peter Wilson, 01520
5	MS 1393	Daniel J. Segalman, 01220
1	MS 9042	James P. Lauffer, 08776
1	MS 9042	Michael D. Jew, 08774
1	MS 9042	Mike Chiesa, 08774
1	MS 0899	Technical Library, 9536 (electronic)

Sandia National Laboratories